PFC/JA-93-24

Quench in Superconducting Magnets, Part II: Analytic Solution

A. Shajii and J.P. Freidberg

January, 1994

Plasma Fusion Center
Massachusetts Institute of Technology
Cambridge, MA 02139 USA

Submitted for publication in: **Journal of Applied Physics**

This work was supported by the US Department of Energy through the Idaho National Engineering Laboratory under contract C88-110982-TKP-154-87. Reproduction, translation, publication, use, and disposal, in whole or in part, by or for the US Government is permitted.

Table of Contents

Abstract

A set of analytic solutions for the Quencher model as described in Part I, is presented in this paper. These analytic solutions represent the first such results that remain valid for the long time scales of interest during a quench process. The assumptions and the resulting simplifications that lead to the analytic solutions are discussed, and the regimes of validity of the various approximations are specified. The predictions of the analytic results are shown to be in very good agreement with numerical as well as experimental results. Important analytic scaling relations are verified by such comparisons, and the consequences of some of these scalings on currently designed superconducting magnets are discussed.

1. Introduction

In this paper we present a set of analytic solutions for the problem of quench propagation in Cable In Conduit Conductors (CICC). The starting point is the Quencher model discussed in Part I [1]. By introducing a series of well justified approximations we first arrive at a simplified quench model (MacQuench) that is well suited for "system studies" because of its high computational speed. Next, after further simplifications, an analytically tractable model describing three different practical regimes of operation is presented. These regimes are denoted by: 1) the "short coil," in which the end-boundaries of the conduit affect the propagation of the quench, 2) the "long coil," in which these end-effects are negligible, and 3) the "small pressure rise regime," in which the helium pressure rise in the quench region remains small. Analytic solutions are derived which distinguish each of these regimes as well as elucidating the basic underlying physics. Furthermore, we verify the validity of the analytic results, in each regime by extensive comparisons with numerical (Quencher and MacQuench) and experimental data.

The MacQuench model simultaneously describes all three regimes and requires only minutes of CPU time per simulation on a Macintosh PC compared to minutes on a CRAY supercomputer for Quencher. The model has much of the flexibility of Quencher (e.g. time dependent current density, time dependent B-field, etc.) and as is shown in the paper, is nearly as accurate, usually to within 5 %. Still, it does require computation and as such is not as convenient or insightful as the analytic theory. Typically, the quantitative accuracy of the analytic theory is $\sim$ 15 % or better. The scaling accuracy of the analytic theory with respect to the physical parameters is excellent in all cases thus far investigated.

The analytic solutions for each of the three regimes are quite distinct. In the short coil, for instance, we find that the quench propagation velocity depends on the length of the conductor L. This dependence is very important when attempting to extrapolate experimental results from short test coil samples to long coils where the quench propagation properties are independent of L. Substantial differences are also observed in the dependence of the quench velocity (V_q) on the current density J. For example, in both the long and the short coil, $V_q \sim J$, while in the low pressure rise coil $V_q \sim J^2$. One common

feature of all three regimes is the inherent dependence of V_q on the initial length of the quench region L_q.

In the past, much of the analytic work on the problem of quench propagation has been carried out by Dresner [2]. In fact, the quench propagation mechanism due to convection of helium, first considered by Dresner, is one of the central assumptions of this paper. Other assumptions made here, however, differ greatly. Dresner's analysis makes use of an elegant similarity solution and is thus applicable to long coils. The specific assumptions introduced in his calculations result in a theory that is valid for relatively short times and low conductor temperatures ($T \lesssim 25$ K). As essentially the only existing analytic results treating the problem of quench in CICC magnets, Dresner's theory is used widely in the superconducting magnet community, although often in regimes where it is inapplicable (i.e. the theoretical assumptions are not satisfied).

In the present work we make use of some of the ideas of Dresner, but introduce an alternate set of approximations that make our solution valid over much longer periods of time (up to and including a full current dump) and higher temperatures ($T \lesssim 300$ K). Our analytic solutions are least accurate for very short times. The present theory is thus complimentary to Dresner's theory.

The main differences in modelling between the two theories of quench propagation are as follows:

a. The contribution of the conductor heat capacity in the quench region is maintained in the formulation presented here. We show this to be the dominant effect in the quench region for long times and high temperatures. For short times the helium heat capacity is dominant and it is this assumption that is made in Dresner's analysis.

b. The dependence of the thermal properties of the conductor are taken into account in the derivation presented here. We believe this is an important ingredient in obtaining quantitative agreements with numerical and experimental results for long times. For short times this is not as critical and thus the material properties are assumed to be constant in Dresner's formulation.

c. As mentioned above, we present analytic solutions in three different regimes of opera-

tion. This is important because for long times qualitatively different types of quench behavior are possible. Dresner's work focuses on the long coil regime since for short times all coils are long coils; that is, there is insufficient time for the end-effects to play a role. The distinction of the various regimes is of central importance in properly interpreting, and extrapolating any experimental results on quench propagation in test coils to large CICC magnets. A detailed comparison of the present results with those of Dresner is made in Section 4 in the discussion of the long coil.

It is worth emphasizing at this point that the MacQuench model and the analytic results apply only to the problem of "classical" quench propagation in CICC, the problem of primary importance to the future large magnets being designed in the magnetic fusion program. The interesting regime of Thermal Hydraulic Quenchback, wherein the temperature ahead of the quench front rises above its critical value, causing a greatly enhanced propagation speed, is not treated here, but is under current investigation.

The remainder of the paper is organized in four sections. In section 2 we briefly review the Quencher model which is discussed extensively in Part I [1]. In section 3 we consider the approximations that lead to a simpler quench model (MacQuench) that is well suited for performing numerical studies on a personal computer. The analytic solution is derived in section 4, and finally in section 5 we present comparisons of the analytic results with numerical and experimental data.

2. Quench Model

Consider quench propagation in Cable In Conduit Conductors (CICC) as described by the compact "Quencher" model presented in Part I [1]. This model, summarized here for convenience, consists of mass and momentum conservation equations for the helium coolant, a hybrid energy equation for the combined helium/conductor, an energy equation for the conduit wall, and an equation of state for the helium. The governing equations are given by

$$\frac{\partial \rho}{\partial t} + \frac{\partial}{\partial x}(\rho v) = 0 \tag{1}$$

$$\frac{\partial p}{\partial x} = -\frac{f \rho v |v|}{2 d_h} \tag{2}$$

$$\rho \hat{C}_t \frac{\partial T}{\partial t} + \rho \hat{C}_h v \frac{\partial T}{\partial x} + \rho \hat{C}_\beta T \frac{\partial v}{\partial x} = \frac{\partial}{\partial x}\left(\kappa \frac{\partial T}{\partial x}\right) + S(T, x, t) + \frac{h P_w}{A_c}(T_w - T) + \frac{A_h}{A_c}\frac{f \rho |v| v^2}{2 d_h} \tag{3}$$

$$p = p(\rho, T) \tag{4}$$

$$\rho_w C_w \frac{\partial T_w}{\partial t} = \frac{h P_w}{A_w}(T - T_w). \tag{5}$$

In Part I it was shown that the corresponding Quencher code accurately describes quench propagation in CICC magnets while saving one to two orders of magnitude in CPU time (i.e. from hours to minutes of CRAY CPU) over existing explicit general purpose magnet design codes. In Part II, several additional, well justified approximations are made, reducing Eqs. (1-5) to the MacQuench model, which requires only several minutes of CPU time on a Macintosh PC. Several further approximations lead to a full analytical solution.

3. The MacQuench Model

The basic insight that allows reduction of the Quencher model is that for the practical cases of interest, quench is propagated by a narrow moving front whose behavior is similar to that of a contact discontinuity. Thus, it is possible to solve the equations separately behind and ahead of the quench front, and then close the model by appropriate matching conditions across the discontinuity. Before proceeding with this analysis, it is helpful to begin with a short discussion of the somewhat subtle initial conditions used in MacQuench.

Initial Conditions

To understand the MacQuench initial conditions, consider first a deliberate, externally excited quench initiation as might be used to test an actual CICC. A magnet of length L operating in its desired superconducting state, is cooled by stagnant supercritical helium to a temperature T_0, pressure p_0, and density ρ_0. A large external heat source ($S_{ext} \gg \eta_{cu} J^2$) is applied over a short length of conductor $L_q (L_q \ll L)$ for a short period of time $t_q (t_q \sim 0.001$ sec). The heat pulse rapidly heats the local temperature above the critical temperature T_{cr}. When S_{ext} is removed, the magnet hot spot is cooled by convection, but heated by $\eta_{cu} J^2$ since this section of magnet is in its normal state. Since $\eta_{cu} J^2 \ll S_{ext}$, the hot spot temperature first decreases due to convection. However, if the initial source S_{ext} was sufficiently large, the joule heating can begin to reheat the hot spot before T falls below T_{cr}. When this occurs, a quench is initiated. The state of the magnet at this point serves as the initial conditions for the MacQuench simulation.

The difficulty in specifying initial conditions lies in the fact that the state of magnet at quench initiation depends upon the details of the initial heating pulse S_{ext}; its magnitude, time duration, spatial length, and spatial profile. A general approach that avoids these difficulties is as follows. First, assume that S_{ext} is experimentally adjusted to the minimum value required to initiate the quench. Under this assumption the initial value for T in MacQuench is given by

$$T(x,0) = (T_q - T_0)\ H(L_q/2 - |x|) + T_0 \tag{6}$$

where $T_q \approx T_{cr}$ and H is the Heaviside step function.

Note that the initial hot spot temperature distribution is chosen to be symmetric and uniform in space. This choice is primarily for simplicity. Tests with other profiles show only a weak sensitivity as long as the total energy input and average profile width are held constant. The quantity L_q in Eq. (6) can usually be set to the length over which the external source is applied. In some experiments, this region can expand slightly because of convection during the short time before quench initiation. If experimental data is available, the measured value of L_q should be used in Eq. (6).

A second initial condition is required for the density. In MacQuench it is assumed that

$$\rho(x,0) = \rho_0. \tag{7}$$

Equation (7) is justified when the external source is applied over such a short period of time, that a negligible amount of density is depleted in the quench region by convection. This corresponds to an external source duration that is much shorter than the characteristic time scale L_q/v. With a typical flow of $v \sim 10$ m/sec and $L_q \sim 1$ m, we find $L_q/v \sim 0.1$ sec. Typically the quench is initiated by sources applied over a period of $\sim 0.001 - 0.01$ sec; thus the aforementioned condition is generally well satisfied in most quench initiation events. From the equation of state we next find the initial helium pressure in the quench region is given by

$$p_q = p(\rho_0, T_q). \tag{8}$$

Observe that in general $p_q > p_0$.

Equations (6) and (7) specify the initial conditions for the helium/conductor in MacQuench. For experimental applications one sets $T_q = T_{cr}$, and assumes that L_q is obtained by direct measurement. For design applications, one sets $T_q = T_{cr}$, and $L_q = L_{qmin}$ where L_{qmin} represents the minimum length in which a quench event can initiate in a CICC. (For typical thermal disturbances that occur during the operation of a magnet the minimum value of the initial quench region may be as small as a fraction of a twist-pitch; that is, $L_{qmin} \sim 1$ cm.) As shown later, these choices correspond to the "worst" case where "worst" is defined as producing the smallest quench detection signal for a given allowable temperature rise in the conductor.

A final initial condition is required for T_w. In MacQuench it is assumed that

$$T_w(x,0) = T(x,0). \tag{9}$$

The heat transfer during the initiation of quench is quite high and this fact coupled with the low specific heat of the conduit wall at low temperatures, causes the equilibration of the two temperatures (helium/conductor and conduit wall) at quench initiation.

Note that the MacQuench initial conditions display discontinuities in the values of T and p, at the locations $x = \pm L_q/2$. These discontinuities, however, are quickly resolved and pose no numerical problems since the system of Eqs. (1-5) is purely diffusive for the density, temperature, and pressure variables.

Quench Region

Having established the initial conditions, we now consider the behavior of the quench region (i.e. the region behind the quench front). A plot of the temperature, pressure, velocity, and density profiles is shown in Fig. 1a–d, respectively. These curves, obtained from a Quencher simulation, correspond to typical profiles in a CICC after the quench has been well established. The location of the quench front is denoted by $X_q(t)$. Within the quench region, $|x| \leq X_q$, the joule heating causes the temperature of the system to increase (Fig. 1a). This in turn increases the helium pressure, (Fig. 1b) inducing a flow of helium in the channel (Fig. 1c). The high temperature helium in the quench region expands against the cold helium ahead of the front, thereby propagating the quench. As shown in Fig. 1d, the expansion causes a depletion of helium density in the quench region, resulting in a compression ahead of the front. The quench front separating the two regions behaves like a moving "contact discontinuity" across which the temperature and density are discontinuous, while the pressure and velocity remain continuous. (The exact nature of the boundary layer, at $x = X_q$ is considered in the discussion of the matching conditions.)

In order to obtain a simple relation for the temperature of the helium/conductor we assume that the CICC is in a uniform magnetic field B. Therefore the joule heating source S in Eq. (5) is independent of x, and is given by $S(T,t) = \eta_c J^2$, where $\eta_c \approx (A_{cu}/A_c)\eta_{cu}(T)$, $J(t) = I(t)/A_{cu}$, and $I(t)$ is the prescribed current in the conductor. Next, note that once the quench is established, the density in the quench region quickly decreases from its initial value ρ_0, while simultaneously the heat capacity of the copper increases in parallel with T. This combination of events, in association with typical values of the quench variables, implies that in the quench region convection, compression, and heat conduction are negligible compared to the time derivative term; that is, the behavior

is dominated by the large heat capacity of the conductor. Equation (3) then assumes a form similar to Eq. (5). The equations for T and T_w thus satisfy

$$\rho\hat{C}_t\frac{\partial T}{\partial t} \approx S(T,t) + \frac{hP_w}{A_c}(T_w - T) \tag{10}$$

$$\rho_w C_w\frac{\partial T_w}{\partial t} = \frac{hP_w}{A_w}(T - T_w). \tag{11}$$

Note that in the quench region the reduced density, and corresponding reduced Reynold's number, cause the heat transfer coefficient h to assume its laminar value; that is $h \approx h(T) = 4d_h/\kappa_h$ where $\kappa_h(T)$ is the thermal conduction of helium. Under this approximation, Eqs. (10) and (11) become ordinary differential equations, implying that with our spatially uniform initial conditions $T(x,t) \rightarrow T(t)$ and $T_w(x,t) \rightarrow T_w(t)$. The appropriate initial conditions are thus $T(0) = T_w(0) = T_q$.

Consider next the density and velocity in the quench region. The low values of density reduce the friction force (proportional to $f\rho v|v|/2d_n$) resulting in a weak pressure gradient. The approximately flat pressure, combined with the spatially homogeneous temperature just discussed, imply that the density profile is also spatially homogeneous; $\rho(x,t) \approx \rho(t)$. This approximation, when substituted into the mass equation [Eq. (1)], leads to a solution for $v(x,t)$ of the form $v(x,t) = (\dot{\rho}/\rho)x$. Furthermore, since the velocity of the quench front $\dot{X}_q$ is carried by the flow of helium it follows by definition that $\dot{X}_q = v(X_q,t)$. These simple relations can be easily manipulated, leading to expressions for ρ and v in terms of $X_q(t)$:

$$v(x,t) = \frac{x}{X_q}\frac{dX_q}{dt} \tag{12}$$

$$\rho(t) = \frac{\rho_0}{2}\frac{L_q}{X_q} \tag{13}$$

where we have used the initial conditions $X_q(0) = L_q/2$ and $\rho(0) = \rho_0$.

The final quantity of interest in the quench region is the pressure. Once the quench is established, the high temperatures ($T \gtrsim 30$K) and low densities ($\rho \lesssim 50$ kg/m^3) imply that the helium equation of state is closely approximated by the ideal gas law. Thus, the pressure is given by

$$p(t) = R\rho T = \frac{\rho_0 R L_q}{2}\frac{T(t)}{X_q(t)}. \tag{14}$$

Equations (10-14) describe the behavior of $T(t), T_w(t), \rho(t)$, and $p(t)$ in terms of $X_q(t)$, a quantity whose dependence is ultimately determined by solving a simplified model ahead of the quench and then matching across the front.

Outer Region

The region ahead of the quench front ($|x| > X_q$) is denoted as the outer region and is characterized by zero joule heating ($S = 0$). Thus the only heat source in this region is due to viscous dissipation ($f\rho v^3/2d_h$). This heating mechanism plays an important role in the initiation of "Thermal Hydraulic Quench-Back" (THQB). Here, viscous heating, together with the heating due to the compression of the helium may raise the temperature in the outer region above $T = T_{cr}$. When this occurs, Joule heating develops almost instantaneously over large segments of the conductor in the outer region. Hence, a rapid increase of the normal zone is observed. The THQB process has been observed in recent experiments, and is a subject of current research. As mentioned in the introduction, the main underlying assumptions of the present paper deliberately exclude the process of THQB. Furthermore, in our studies the viscous dissipation in the outer region only slightly effects the quench propagation in the "classical" (non-THQB) regime, the most common quench regime in a CICC. Thus in the following analysis we neglect the viscous dissipation term in the outer region.

In view of the above discussion, consider first the temperature. In the outer region the value of the heat transfer coefficient h is very large ($h \sim 5000$ W/m-K) due to substantial helium flow velocities ($\sim$ 5 m/sec) and the high density of helium ($\rho \sim 150$ kg/m^3). The large heat transfer between the helium and the conduit wall results in temperature equilibration ($T_w \approx T$). By appropriately adding Eqs. (3) and (5), such that the heat transfer term, $h(T - T_w)$ is cancelled, and setting $T_w = T$, we obtain a single energy equation in the outer region. The result is identical to Eq. (3), except the total specific heat, $\hat{C}_t$ now includes the contribution of the conduit wall: $\rho\hat{C}_t \rightarrow \rho_c C_c + (A_h/A_c)\rho C_h + (A_w/A_c)\rho_w C_w$. Even so, the high density and low temperature of the helium causes the helium contribution to dominate the specific heat so that $\rho\hat{C}_t \approx (A_h/A_c)\rho C_h$. Also, as

seen in Fig. 1a–d, the spatial gradients are weak, implying that the heat conduction term is negligible. Combining these results leads to the following equation for the temperature in the outer region

$$\frac{\partial T}{\partial t} + v\frac{\partial T}{\partial x} + (C_\beta/C_h)T\frac{\partial v}{\partial x} = 0. \tag{15}$$

An alternate form of Eq. (15), obtained from the conservation of mass and the definitions of C_β and C_h, is given by $d\hat{S}/dt = 0$ where $\hat{S}$ is the entropy. Thus, $\hat{S}(\rho, T) = \hat{S}(\rho_0, T_0) =$ const. in the outer region.

The density can be related to the temperature by eliminating $\partial v/\partial x$ from Eq. (15) by means of the conservation of mass. The result is

$$\frac{dT}{d\rho} = \frac{T}{\rho}\frac{C_\beta(T,\rho)}{C_h(T,\rho)}. \tag{16}$$

Equation (16) can easily be solved numerically by assuming $T = T_0$ when $\rho = \rho_0$ and we shall hereafter assume that $T = T(\rho)$ is a known function.

The next step is to obtain a relationship between v and ρ. Consider $p = p(\rho, \hat{S})$ with $\hat{S} = \hat{S}_0 =$ const. The momentum equation then yields the following expression for v

$$v = \left(\frac{2d_h}{f}\right)^{1/2}\left(-\frac{c^2}{\rho}\frac{\partial \rho}{\partial x}\right)^{1/2} \tag{17}$$

where $c^2(\rho, \hat{S}_0) = (\partial p/\partial \rho)_{\hat{S}_0}$ is the square of the sound speed. Note that in this equation we assume the friction factor f is a constant. This assumption is well justified because of the weak dependence of f on the Reynold's number ($f \propto 1/R^{0.2}$). The final results are not strongly dependent on f, and using a constant value of $f \approx 0.06 - 0.08$ is a good approximation for the friction factor in the outer region.

At this point the velocity and temperature are expressed in terms of the helium density ρ in the outer region. The final relation that determines ρ is obtained by substituting v, given by Eq. (17), into the mass equation. The resulting equation is given by

$$\frac{\partial \rho}{\partial t} + \left(\frac{2d_h}{f}\right)^{1/2}\frac{\partial}{\partial x}\left(-c^2\rho\frac{\partial \rho}{\partial x}\right)^{1/2} = 0 \tag{18}$$

which is a nonlinear diffusion equation requiring one initial and two boundary conditions. The initial condition is $\rho(x, 0) = \rho_0$, where ρ_0 is the initial density of the stagnant helium.

The boundary condition at $x = L/2$ is given by $\rho(L/2,t) = \rho_0$ and is consistent with the constant pressure boundary condition discussed in Part I [1]. The second boundary condition is specified at the quench front $X_q(t)$, and follows from the matching conditions discussed shortly. Note that the treatment of the outer region is reduced to solving a single parabolic partial differential equation.

Matching Conditions

In order to mathematically close the MacQuench model two additional conditions are required; one for the remaining boundary condition on Eq. (18) and one to determine the location of the quench front $X_q(t)$. These are obtained by noting that the quench front behaves like a contact discontinuity satisfying certain jump conditions. We start by moving to the quench front reference frame and then integrating the mass equation. The result is

$$\frac{dX_q}{dt} = \frac{[\![\rho v]\!]}{[\![\rho]\!]} \tag{19}$$

where $[\![Q]\!]$ denotes $Q(X_q^+,t) - Q(X_q^-,t)$. In order to avoid the formation of a shock in the conduit we require $[\![v]\!] = 0$. Equation (19) then automatically becomes consistent with Eq. (12). Since the velocity is continuous across $x = X_q$, equating Eqs. (17) and (19), leads to the first matching condition;

$$\frac{dX_q}{dt} = \left(\frac{2d_h}{f}\right)^{1/2} \left(-\frac{c^2}{\rho}\frac{\partial \rho}{\partial x}\right)^{1/2}\Bigg|_{x=X_q^+}. \tag{20}$$

This equation relates the location of the quench front to the density profile in the outer region (specifically X_q is determined by the value of ρ and $\partial\rho/\partial x$ at $x = X_q^+$).

The second matching condition is obtained by integrating the momentum equation across the moving quench front yielding

$$[\![p]\!] = 0. \tag{21}$$

This relation states that helium pressure is continuous across $x = X_q$. A more convenient form of Eq. (21) can be written as

$$\frac{\rho_0 R L_q}{2}\frac{T}{X_q}\Bigg|_{X_q^-} = p(\rho,\hat{S}_0)\Bigg|_{X_q^+}. \tag{22}$$

Equations (20) and (22) determine the location of the quench front and the remaining boundary condition on ρ, respectively

Observe that the MacQuench model is now closed. However, we have yet to use the jump condition information from the energy equation. An analysis of the energy equation [3] shows that integrating across the front does not impose any constraints on the temperature jump, but instead determines the width of the layer. Specifically, in reference [3] it is shown that in the layer

$$T(x,t) \approx T(X_q^+,t) + [T(X_q^-,t) - T(X_q^+,t)]e^{-(x-X_q^-)/\Delta} \tag{23}$$

where $\Delta(t) \approx \kappa(T_0)/\dot{X}_q \rho_c C_c(T_0)$. For typical experimental values $\Delta \lesssim 0.20$ m, a value similar to those observed in Quencher simulations. Note that in the entire MacQuench model, the conductor thermal conductivity only plays a role in the quench front layer, determining its width. As in many fluid dynamic boundary layer problems, this implies that most of physically observable quantities of interest are independent of κ. This too is born out in Quencher simulations.

The MacQuench Model

To summarize, the final simplified MacQuench model reduces to a set of equations determining $T(t), T_w(t)$ in the quench region, $\rho(x,t)$ in the outer region, and the front location $X_q(t)$. These have the form

$$\rho \hat{C}_t \frac{dT}{dt} = \eta_c J^2(t) + \frac{hP_w}{A_c}(T_w - T) \tag{24}$$

$$\rho_w C_w \frac{dT_w}{dt} = \frac{hP_w}{A_w}(T - T_w) \tag{25}$$

$$\frac{\partial \rho}{\partial t} = -\left(\frac{2d_h}{f}\right)^{1/2} \frac{\partial}{\partial x}\left(-c^2 \rho \frac{\partial \rho}{\partial x}\right)^{1/2} \tag{26}$$

$$\frac{dX_q}{dt} = \left(\frac{2d_h}{f}\right)^{1/2} \left(-\frac{c^2}{\rho}\frac{\partial \rho}{\partial x}\right)^{1/2}_{X_q^+}. \tag{27}$$

The corresponding initial and boundary conditions are given by

$$T(0) = T_w(0) = T_q \tag{28}$$

$$\rho(x,0) = \rho(L/2,t) = \rho_0 \tag{29}$$

$$p[\rho(X_q,t),\hat{S}_0] = \frac{\rho_0 R L_q}{2}\frac{T(t)}{X_q(t)} \tag{30}$$

$$X_q(0) = L_q/2. \tag{31}$$

In the quench region it is assumed that $C_c(T), \eta_c(T), h(T)$, and $C_w(T_w)$ are known property functions. Similarly, in the outer region $\hat{S}_0 = \hat{S}(\rho_0, T_0), c^2(\rho, \hat{S}_0)$, and $p(\rho, \hat{S}_0)$ are assumed to be known properties of supercritical helium.

The numerical solution of the MacQuench model consists of solving the ODE's given by Eqs. (24), (25), (27), and the diffusion equation (26). The ODE's are standard. The diffusion equation is solved by approximating the partial time derivative $\partial/\partial t$, in Eq. (26) by a second order accurate finite difference scheme, and solving the resulting boundary value problem by standard techniques. The treatment of Eq. (26) is similar to the Quencher model, discussed in Part I [1]. This numerical procedure requires only few minutes of CPU time on a Macintosh PC. In section 5 we present detailed comparisons of the MacQuench model with the solution of Eqs. (1–5).

4. Analytic Solution

This section presents a derivation of an approximate analytic solution to the MacQuench model. By making several additional plausible assumptions, it is possible to obtain solutions in both the quench and outer regions in terms of $X_q(t)$. Matching across the quench front then leads to a single ODE for the quantity $X_q(t)$. In its initial form this equation is still too complicated to solve analytically. However, by considering several special limits we obtain explicit analytical solutions as well as the boundaries in parameter space that define each regime.

The specific goals of the analysis are to calculate $T(t)$ in the quench region and $X_q(t)$. All other quantities of interest can be easily obtained by simple subsidiary relations. Throughout the following analysis, unlike the MacQuench model, we assume that the current density J is constant in time.

Quench Region

Equations (24) and (25) for $T(t)$ and $T_w(t)$ determine the temperature in the quench region. Recall that helium depletion has led to the approximation $\rho\hat{C}_t \equiv \rho_c C_c + \rho\hat{C}_h \approx \rho_c C_c$ in Eq. (24). Thus, these two equations are a set of closed, coupled ODE's for the unknowns T and T_w. In most situations of interest, the heat transfer coefficient is reasonably high so that the temperature difference is not very large: $(T - T_w)/T < 1$. Exploiting this fact we introduce new variables

$$\overline{T} = \frac{1}{2}(T + T_w) \tag{32}$$

$$\Delta T = \frac{1}{2}(T - T_w) \tag{33}$$

and for mathematical simplicity assume $\Delta T \ll \overline{T}$. Equations (24) and (25) are added to cancel the heat transfer terms. Neglecting the remaining ΔT terms leads to a single equation for the average temperature

$$\frac{d\overline{T}}{dt} = \alpha(\overline{T})J^2 \qquad \overline{T}(0) = T_q \tag{34}$$

where

$$\alpha(\overline{T}) = \frac{A_{cu}\eta_{cu}(\overline{T})}{A_c\rho_c C_c(\overline{T}) + A_w\rho_w C_w(\overline{T})}. \tag{35}$$

For CICC magnets, the temperature dependence of $\alpha(\overline{T})$ can be approximated by

$$\alpha(\overline{T}) \approx \alpha_0(1 + \overline{T}^2/T_\eta^2)^{1/2}. \tag{36}$$

The quantity α is constant out to T_η after which it increases linearly with $\overline{T}$. The parameters α_0 and T_η are functions of the conduit material (e.g. stainless steel, aluminum) and the area ratio A_w/A_c. Typically $\alpha_0 \sim 5 \times 10^{-16}$ m^4-K/A^2-sec, $T_\eta \sim 100$K. A simple, practical, and reasonably accurate method to determine α_0 is to set $\alpha_0 = \alpha_{min}$, where α_{min} is

the minimum value of $\alpha(\overline{T})$. Figure 2 demonstrates the accuracy of this approximation for the proposed ITER toroidal magnet characterized by $A_w/A_c = 0.39$, $A_{cu}/A_c = 0.61$, and assuming a stainless steel wall (here $\alpha_0 = 7 \times 10^{-16}$ m^4-K/A^2-sec and $T_\eta = 100$ K). Note that this approximation breaks down at lower temperatures ($\lesssim$ 20 K) where the specific heat of the solid components is small. However, the approximation given by Eq. (36) does not result in large errors in predicting the temperature for two reasons; first, the actual value of α in the low temperature regime includes the contribution of the helium specific heat in the denominator of Eq. (35). This contribution tends to lower the value of α in this regime. In Fig. 2 we also plot α including the specific heat of helium as obtained from Quencher during a typical quench simulation. Note that as the temperature increases the helium contribution to α diminishes. Secondly, in this regime, the temperature increases very rapidly since α is large. Thus in a very short period of time Eq. (36) becomes a good approximation to α.

Using Eq. (36) in Eq. (34) and assuming J to be constant (no current dump) yields an ODE that can be easily integrated. The result is

$$\overline{T} = T_\eta \sinh\left[\frac{\alpha_0 J^2}{T_\eta}(t + t_\eta)\right] \approx T_q + \alpha_0 J^2 t \tag{37}$$

where t_η satisfies $\sinh(\alpha_0 J^2 t_\eta / T_\eta) = T_q/T_\eta$. For large CICC magnets, typically $t_\eta \sim 0.5$ sec. The approximate form is valid for $\overline{T} \lesssim T_\eta$, which is the usual situation of interest.

From Eq. (37) one can easily calculate $\Delta T(t)$. After a short calculation in which the heat transfer coefficient is assumed large, we obtain

$$\Delta T(t) \approx \frac{A_w \rho_w C_w}{2hP_w}\alpha(\overline{T})\ \left(1 - e^{-t/\tau_w}\right) \tag{38a}$$

where

$$\frac{1}{\tau_w} = hP_w\left(\frac{1}{A_c\rho_c C_c} + \frac{1}{A_w\rho_w C_w}\right) \tag{38b}$$

and all coefficients are evaluated at $T = \overline{T}(t)$.

The final quantity of interest is the helium pressure. In the quench region the temperature rises and the helium density is quickly depleted. As a consequence, the helium

equation of state can be accurately approximated by that of an ideal gas. Thus, shortly after the quench has been initiated $p \approx R\rho(\overline{T} + \Delta T)$. With ρ given by Eq. (13), the pressure can be expressed as

$$p(t) = \frac{R\rho_0 L_q}{2}\left(\frac{\overline{T} + \Delta T}{X_q}\right). \tag{39}$$

Equations (37-39) provide analytic expressions for the quench variables in terms of the unknown function $X_q(t)$.

Outer Region

The expansion of the high temperature helium behind the quench causes a compression of the helium in the outer region. Because of the large volume of the outer region, and the supercritical state of the helium in this region the compression causes only a slight increase in the density and temperature above their background values. Consequently, ρ and T can be accurately approximated by

$$\rho(x,t) \approx \rho_0 + \rho_1(x,t) \tag{40a}$$

$$T(x,t) \approx T_0 + T_1(x,t) \tag{40b}$$

where $\rho_1 \ll \rho_0$ and $T_1 \ll T_0$. Substituting this expansion into Eq. (16) leads to a simple relationship for T_1 in terms of ρ_1 given by

$$T_1(x,t) = \left[\frac{T_0 C_\beta(\rho_0, T_0)}{\rho_0 C_h(\rho_0, T_0)}\right]\rho_1(x,t). \tag{41}$$

Similarly, the pressure in the outer region can be expressed in terms of ρ_1 by expanding the equation of state

$$p(x,t) \approx p_0 + c_0^2\rho_1(x,t). \tag{42}$$

where $c_0^2 = c^2(\rho_0, \hat{S}_0)$.

The next step is to solve for ρ_1 from the simplified form of Eq. (26), which can be written as

$$\frac{\partial \rho_1}{\partial t} = -\nu_0 \frac{\partial}{\partial x}\left(-\frac{\partial \rho_1}{\partial x}\right)^{1/2}. \tag{43a}$$

Here,

$$\nu_0 = \left(2d_h\rho_0 c_0^2/f\right)^{1/2}. \tag{43b}$$

With little loss of accuracy, f can be assumed constant at $f \approx 0.07$. Note that even though $\rho_1/\rho_0 \ll 1$, the equation for ρ_1 remains nonlinear.

Equation (43a) does not have a simple analytical solution. However, an approximate solution can be obtained by transforming to similarity coordinates as follows: $\tau = t, \xi = (x - L_q/2)/t^{2/3}$. Equation (43a) becomes

$$\tau\frac{\partial\rho_1}{\partial\tau} - \frac{2}{3}\left(\xi\frac{\partial\rho_1}{\partial\xi}\right) = -\nu_0\frac{\partial}{\partial\xi}\left(-\frac{\partial\rho_1}{\partial\xi}\right)^{1/2}. \tag{44}$$

For the moment assume $\partial\rho_1/\partial\tau = 0$. Then Eq. (44) has a pure similarity solution given by

$$\frac{\partial\rho_1}{\partial\xi} = -\frac{9\nu_0^2}{(K+\xi^2)^2} \tag{45}$$

where K is an integration constant.

If the boundary conditions could be satisfied with $K = \text{const}$, then Eq. (45) would be the exact solution to the problem. This is not the case. However, in the analysis that follows it is shown that Eq. (45) is an approximate solution to the problem in the sense that the K required to satisfy the boundary conditions is a slowly varying function of time: $K = K(\tau)$. Under this assumption, the outer region solution is given by Eqs. (41), (42) and (45) with $K(\tau)$ an as yet undetermined function.

Matching Conditions

The system of equations is closed by applying the matching conditions. Consider first the pressure balance jump condition given by Eq. (30). The quench region pressure at $x = X_q^-$ has been calculated in Eq. (39). The outer region pressure at any x follows from integrating Eq. (45), assuming $\rho_1(L/2,t) = 0$, and then substituting into Eq. (42). Setting $x = X_q^+$ and balancing the pressures leads to

$$\frac{\rho_0 RL_q}{2}\left(\frac{\overline{T}+\Delta T}{X_q}\right) = p_0 + 9\nu_0^2 c_0^2 t^2 \int_{X_q}^{L/2} \frac{dx}{\left[(x - L_q/2)^2 + X_D^2\right]^2} \tag{46}$$

where $X_D(t) = t^{2/3}K^{1/2}$ represents the location of the leading edge of the diffusion front. In general $X_D \gg X_q$. This is the first of the expressions relating the two unknowns $X_q(t)$ and $X_D(t)$.

The second relation follows from the velocity jump condition described by Eq. (27). A simple calculation, again making use of Eq. (45) yields

$$\frac{dX_q}{dt} = \frac{3\nu_0^2}{\rho_0} \frac{t}{(X_q - L_q/2)^2 + X_D^2}. \tag{47}$$

Equations (46) and (47) represent a closed model for the unknowns $X_q(t)$ and $X_D(t)$. In its present form the model is still too difficult to solve analytically. However, there are several special limits in which explicit analytic solutions can be obtained. These are the "short coil", the "long coil", and the "low pressure rise regime", which are discussed next.

Short Coil

To decide whether a given coil is "short" or "long" one must compare two different time scales. First there is the nonlinear diffusion time t_D, determined from the solution of Eq. (43a). For $t < t_D$ (or equivalently $X_D < L/2$) end effects are unimportant. Conversely for $t > t_D$. The second time scale is defined as the characteristic time required for the temperature in the conductor to rise to some maximum allowable value T_m. This time is easily estimated from Eq. (37) and is defined by $t_m \equiv T_m/\alpha_0 J^2$. When the time scale of interest exceeds the diffusion time ($t_m > t_D$) the magnet behaves like a short coil. In the discussion that follows, analytic solutions are presented for the short coil regime as well as an explicit criterion for the critical coil length defining the region of validity.

The analysis begins by recognizing that the short coil limit corresponds to the assumption $(L/2)^2 \ll X_D^2(t_m)$ in Eq. (46), thus allowing us to neglect the $(x - L_q/2)^2$ term in the integrand. We further assume that $X_q \ll L/2$ (i.e. the quench front at $t = t_m$ is still some distance away from the end of the coil) and use the approximate form for $\overline{T} \approx T_q + \alpha_0 J^2 t$, valid for $T_m \lesssim T_\eta$. Also, in both the short and long coil limits we find X_q is weakly dependent on the helium temperature T, and thus ΔT. This, together with the relation $\Delta T < \overline{T}$, justifies neglecting ΔT in Eq. (46) (this assumption is not used in the

low pressure rise regime, since there X_q is linearly dependent on ΔT). Similarly, once the quench is initiated, the pressure behind the quench front usually greatly exceeds the initial pressure ahead of the front, thereby allowing us to neglect the p_0 term in Eq. (46) (when this is not the case we have the low pressure rise regime which is discussed separately). These approximations yield the following expression for $X_D(t)$ as a function of $X_q(t)$

$$\frac{t^2}{X_D^4} \approx \frac{\rho_0 R L_q}{9\nu_0^2 c_0^2 L}\left(\frac{\alpha_0 J^2 t}{X_q}\right). \tag{48}$$

The expression given by Eq. (48) is to be substituted into Eq. (47). The resulting equation can be simplified by assuming $X_q^2 \ll X_D^2$ in the denominator, an assumption that is well satisfied for the short coil (except for t very close to zero) since $X_q^2 \ll (L/2)^2 \ll X_D^2(t_m)$. The end result is a single equation for $X_q(t)$ given by

$$\frac{dX_q}{dt} \approx \left(\frac{2d_h R L_q}{fL}\right)^{1/2}\left(\frac{\alpha_0 J^2 t}{X_q}\right)^{1/2}. \tag{49}$$

The solution, valid once the quench is well initiated, ($X_q \gg L_q/2$) has the from

$$X_q = \left[(L_q/2)^{3/2} + (V_q\, t)^{3/2}\right]^{2/3} \tag{50}$$

$$V_q = \left(\frac{2d_h R}{fL}\, L_q \alpha_0 J^2\right)^{1/3}. \tag{51}$$

The coefficient V_q is the asymptotic quench velocity and is an important quantity of experimental interest.

Equation (51) shows that in a short coil, the quench front propagates with a constant velocity. Observe that V_q is a function of the product $L_q J^2$. Small L_q and/or J lead to a slow quench velocity V_q. Since T in the quench region is independent of L_q, a very localized quench initiation (i.e. small L_q) leads to a small V_q for a given temperature rise, thereby increasing the difficulty of detection. Note that V_q is a weak function of L: $V_q \propto L^{-1/3}$. Since end effects are important in a short coil it is not surprising that $V_q = V_q(L)$.

Knowing X_q, we can substitute back into the expression for K. The result is $K(t) \approx (3\nu_0^2/\rho_0 V_q)t^{-1/3} \propto t^{-1/3}$ which is relatively slowly varying. The value of $K(t_m)$ can next

be inserted into the inequality criterion defining the regime of validity for the short coil $[(L/2)^2 \ll X_D^2(t_m)]$. We conclude that a CICC is a short coil if

$$L^2 \ll \frac{24 d_h c_0^2 t_m}{f V_q}. \tag{52}$$

Thus, the short coil limit corresponds to the steady state solution of Eq. (43a), with ρ_1 and v given by

$$\rho_1(x,t) = \left(\frac{\rho_0 f V_q^2}{2 d_h c_0^2}\right)\left(\frac{L}{2} - x\right) \tag{53a}$$

$$v(x,t) = V_q. \tag{53b}$$

Observe that the density decreases linearly with x while the velocity is a constant. This is the expected behavior in situations where the time scale of interest is sufficiently long to allow the profiles to come into a quasi-static equilibrium with respect to the diffusive processes.

Long Coil

Most of the large CICC magnets currently being designed can be characterized as "long coils." In terms of the basic analytical model given by Eqs. (46) and (47) a long coil is defined by the two criteria $(L/2)^2 \gg X_D^2(t_m)$ and $X_q^2 \ll X_D^2(t_m)$. Physically this corresponds to $X_q \ll X_D \ll L/2$: the location of the diffusion edge (X_D) at the time of interest (t_m) is well short of reaching the end of the coil $(L/2)$ but is far ahead of the quench front (X_q). Under this definition the limits of integration in Eq. (46) transform from $(X_q, L/2)$ to $(0, \infty)$. Note that replacing X_q by 0 is consistent with the long coil assumption except for t very close to zero.

If we again assume $\overline{T} \lesssim T_\eta$, Eq. (46) can be easily integrated yielding an expression for X_D in terms of X_q

$$\frac{t^2}{X_D^3} \approx \frac{2}{9\pi} \frac{\rho_0 R L_q}{\nu_0^2 c_0^2} \left(\frac{\alpha_0 J^2 t}{X_q}\right). \tag{54}$$

Equation (54) is substituted into Eq. (47), where, as for the short coil, we assume $X_q^2 \ll X_D^2$. The resulting equation for X_q has the form

$$\frac{dX_q}{dt} \approx 3\left(\frac{2}{9\pi}\right)^{2/3}\left(\frac{2d_h R^2 L_q^2}{f c_0^2}\right)^{1/3}\left(\frac{\alpha_0 J^2 t}{X_q}\right)^{2/3}\left(\frac{1}{t}\right)^{1/3}. \tag{55}$$

This equation can be easily solved yielding

$$X_q = \left[(L_q/2)^{5/3} + (V_q\ t)^{5/3}\right]^{3/5} \tag{56}$$

where the asymptotic quench velocity is given by

$$V_q(t) = 0.766\left(\frac{2d_h}{f}\right)^{1/5}\left(\frac{RL_q\alpha_0 J^2}{c_0}\right)^{2/5}\frac{1}{t^{1/5}}. \tag{57}$$

Note that for convenience we have defined $V_q \equiv (5/4)\dot{X}_q$.

Observe that V_q has a similar qualitative behavior with $L_q J^2$ as for the short coil. However, V_q decreases slowly with time: $V_q \propto t^{-1/5}$. In comparing short and long coils we see that some of the scaling is quite different. In particular, there is, as expected, no dependence on L in the long coil.

Consider next the evaluation of $K(t)$. Substituting back into Eq. (54) yields $K(t) \approx (3\nu_0^2/\rho_0 V_q)t^{-1/3}$, $K \propto t^{-2/15}$. The slow K approximation is very plausible. The criteria defining the regime of the long coil $(L/2)^2 \gg X_D^2(t_m)$ and $X_q^2 \ll X_D^2(t_m)$ can now be expressed as

$$L^2 \gg \frac{24 d_h c_0^2 t_m}{f V_q} \gg 4V_q^2 t_m^2. \tag{58}$$

Equation (58) is well satisfied for many large CICC magnets.

The final quantities of interest are the profiles for ρ_1 and v in the outer region. These are easily extracted from the analysis and are given by

$$v(x,t) = \frac{V_q\ t}{t + \lambda_1^2(x - L_q/2)^2} \tag{59a}$$

$$\rho_1(x,t) = \frac{9\nu_0^2}{2K^{3/2}}\left(\cot^{-1}\frac{\xi}{K^{1/2}} - \frac{K^{1/2}\xi}{K+\xi^2}\right) \approx 3\nu_0^2\ \frac{\lambda_2^3\ t^2}{[t^{1/2} + \lambda_2(x - L_q/2)]^3} \tag{59b}$$

where $\lambda_1^2(t) = \rho_0 V_q / 3\nu_0^2$ and $\lambda_2(t) = (3\pi/4)^{1/3}\lambda_1$. As expected, in a long coil both the velocity and density profiles decay for large x and spread in width as time progresses. An important quantity of interest during a quench in long coils is the helium expulsion velocity from the conduit. In accord with the long coil limit we find, from Eq. (59a), that the expulsion velocity is given by

$$v(x = L/2, t) \approx \frac{24 d_h c_0^2}{f L^2}\, t. \tag{59c}$$

At this point we can make a direct comparison between the long coil solution presented above, and the analytic solution given by Dresner. To begin, we summarize Dresner's results for $T(t)$, $p(t)$ and $V_q(t)$;

$$T_D(t) = \frac{0.10}{R\rho_0 L_q}\left(\frac{4d_h}{f\rho_0^2 c_0^2}\right)^{1/3} (\eta_0 J^2)^{5/3}\, t^{7/3} \tag{60}$$

$$p_D(t) = 0.21\, \eta_0 J^2\, t \tag{61}$$

$$V_{qD} \equiv \frac{5}{4}\,\dot{X}_q = 0.42\,\left(\frac{4d_h}{f\rho_0^2 c_0^2}\right)^{1/3} (\eta_0 J^2)^{2/3}\, t^{1/3} \tag{62}$$

where we use the subscript D to denote Dresner's results. All variables have been defined previously except η_0. This quantity represents the resistivity of the copper which is assumed to be constant. It makes little sense to attempt a quantitative comparison between these equations and the long coil solution presented in this paper, since the two sets of results are inherently based on very different assumptions. This fact is evident in the large qualitative differences in the scalings of T, p, and V_q with t between the two sets of solutions.

Specifically, consider the following. In Eq. (60) the contribution of the conduit wall has not been included. Thus, this equation should be compared with Eq. (37), with $\Delta T = 0$ which results in $\overline{T} = T$. Next, Eq. (61) describes the maximum helium pressure in the quench region. For the assumptions used in Dresner's derivation, this equation is to be compared with Eq. (39) in the following form

$$p(t) = 0.653\left(\frac{f c_0^2}{2d_h}\right)^{1/5} (R\rho_0 L_q)^{3/5}\, (\alpha_0 J^2)^{3/5}\, t^{1/5}.$$

Finally, Eq. (62) should be compared with Eq. (57). Again, the qualitative differences are apparent. The only parameter that is the same in both theories is the helium expulsion velocity. The expulsion velocity obtained by Dresner is the same as Eq. (59c). This is a consequence of assuming an infinite conductor length and thus discarding all information from the quench region, when considering $x = L/2$.

"Small Δp" Regime

The last regime of interest corresponds to the case in which the pressure rise Δp in the quench region remains small. This regime corresponds to the limit of a "weak" quench. When the current density is low, the frictional force small, or the quench initiation length short, the helium coolant easily removes the quench generated heat, leaving the pressure in the quench region only slightly higher than the background value. From the previous analysis it follows that the condition to lie in the small Δp regime is approximately given by

$$\frac{R\rho_0}{2p_0}\frac{\alpha_0 L_q J^2}{V_q} \ll 1. \tag{63}$$

Most quench events in large CICC magnets violate this condition (i.e. $p(t_m)/p_0 \gg 1$). However, the experiment of Ando et al. [4] discussed in Part I lies in the small Δp regime.

When Δp is small the quench pressure can be expressed as $p = p_0 + p_1(t)$, with $p_1/p_0 \ll 1$. Using this relation on the right-hand side of Eq. (46) allows us (to leading order in p_1/p_0) to neglect the integral contribution. Thus, $X_q \approx R\rho_0 L_q(\overline{T} + \Delta T)/2p_0$. In order to match the initial condition we add a small first order constant, yielding

$$X_q \approx R\rho_0 L_q(\overline{T} + \Delta T - T_q)/2p_0 + L_q/2. \tag{64}$$

For the case where $\Delta T \ll \overline{T}$, and $\overline{T} \lesssim T_\eta$, we find $V_q \equiv \dot{X}_q \approx R\rho_0 L_q \alpha_0 J^2/2p_0$. Note the strong dependence of the quench velocity on J. This dependence is much stronger than in the short and long coils. For $T > T_\eta$, X_q increases exponentially with J^2. Also, Eq. (64) is valid for the entire temperature range (20-300 K), while in deriving Eqs. (51) and (57) we assumed $\overline{T} \lesssim T_\eta$. Interestingly, the propagation of quench in the "small Δp" regime is independent of the thermal hydraulics of the helium in the conduit.

Next, we proceed to obtain the first order pressure rise $p_1(t)$. From the first order part of Eq. (46) we find

$$p_1(t) = 9\nu_0^2 c_0^2 t^2 \int_{X_q}^{L/2} \frac{dx}{[(x - L_q/2)^2 + X_D^2]^2} \tag{65}$$

where for both the long and the short coils, from Eq. (47) we have

$$X_D^2 = \frac{3\nu_0^2}{\rho_0} \frac{t}{V_q}. \tag{66}$$

In order to evaluate the integral in Eq. (65) we consider the two limits given by Eqs. (52) and (58), respectively. For the short coil we find

$$p_1(t) = \left(\frac{f\rho_0 L}{4d_h}\right) V_q^2. \tag{67}$$

Similarly for the long coil we obtain

$$p_1(t) = 1.36 \left(\frac{f}{2d_h}\right)^{1/2} \rho_0 c_0 \, t^{1/2} V_q^{3/2} \tag{68}$$

where $V_q(t) = \dot{X}_q$ is obtained from Eq. (64). Just as in the long and short coil limits, we may obtain the solution for $\rho_1(x,t)$ and $v(x,t)$ in the outer region from Eqs. (17) and (45).

5. Discussion

In the discussions that follow, we provide detailed comparisons of the Quencher, Mac-Quench and Analytic models, as well as comparisons with experimental data.

Long Coil

We consider a conductor of length 530 m, similar to the TF coil of ITER. The parameters describing this conductor are $A_h = 4.5 \times 10^{-4}$ m^2, $A_{cu} = 3.9 \times 10^{-4}$ m^2, $A_{sc} = 2.5 \times 10^{-4}$ m^2, $A_w = 2.5 \times 10^{-4}$ m^2, $P_w = 0.13$ m, and $d_h = 5 \times 10^{-4}$ m. The transport current is $I = 43$ kA and the conductor is assumed to be in a constant magnetic field of 13 T. Before the initiation of quench, the stagnant helium in the channel is at a temperature of 5 K, and a pressure of 5 atm. Two quench scenarios are investigated. In scenario (1) $L_q = 3$ m while in scenario (2) $L_q = 8$ m. The studies have three goals: first, to compare the accuracy of the different models in the long coil regime, second to determine quantitatively the effect of quench initiation length L_q on quench propagation, and third to ascertain the accuracy of the analytic scaling relations with I.

In Fig. 3a–d we compare the cable temperature $T = \overline{T} + \Delta T$, the normal length $2X_q$, the quench helium pressure p, and the helium expulsion velocity $v(x = L/2, t)$, respectively, as obtained by the various models during a 6 second quench. The analytic results are given by Eqs. (32–38), (39), (56–57), and (59c) with $\alpha_0 = 7 \times 10^{-16}$ m^4-K/A^2-sec, $J = 1.1 \times 10^8$ A/m^2, $T_\eta = 100$ K, $T_q = 10$ K, $R = 2080$ J/kg-K, $\rho_0 = 130$ kg/m^3, $c_0 = 215$ m/sec, and $f = 0.07$. In Fig. 3a, only case (1) is presented, since less than ~ 6 % difference in T between the two scenarios was found. The dependence of the normal length and the helium pressure on L_q is evident in Figs. 3b and 3c, where we observe good agreement between the various models. Finally, in Fig. 3d we compare the helium expulsion velocity as obtained by Quencher, MacQuench and Eq. (59c). Only the case $L_q = 3$ m is presented since less than ~ 1 % difference was observed between the two scenarios. Note that the six second quench simulation observed in these figures took approximately 4 hours of CPU time on a Vax 4000/90 with Quencher, while less than 2 minutes of CPU time was used by MacQuench on the same machine (this is equivalent to less than 10 minutes of CPU time on a Macintosh Centris 650).

Consider now the dependence of the average temperature $\overline{T}$, and the normal length on the transport current I. In Fig. 4 we plot $(\overline{T} - T_q)$ and $2X_q$ each evaluated at $t = 4$ sec versus the square of the transport current I^2. We have normalized these quantities

such that $A \equiv (\overline{T} - T_q)/(\overline{T} - T_q)_r$ and $B \equiv (X_q)/(X_q)_r$, where the subscript r denotes the value of the relevant quantities at the reference $I = I_r = 30$ kA. In this figure we compare A and B as obtained by Quencher, MacQuench and the analytic results. From Eqs. (37), (56) and (57), in the regime $\overline{T} \lesssim T_\eta$ (which is the case for all the points in Fig. 4) we have $A \propto I^2$ and $B \propto I^{4/5}$, which is clearly observed in Fig. 4.

Short Coil

One of the most distinct differences between the long and the short coil is the dependence of the quench velocity on the coil length L. In the short coil regime $X_q \propto L^{-1/3}$, while the long coil solution of X_q is independent of L (see Eqs. (51) and (57)). This dependence is important in designing and interpreting results from experiments carried out on shorter, less expensive test coil samples. Care must be exercised to guarantee that the test coil does not inadvertently operate in the short coil regime, while the actual coil of interest lies in the long coil regime. Such a difference could lead to erroneous extrapolations, particularly with respect to X_q. One of the main goals of the short coil studies is to quantify this issue.

We consider a 4 sec quench scenario in a 50 m long sample of the ITER conductor just described. The initial quench length is assumed to be $L_q = 3$ m. First, note that using the relevant parameters discussed above in Eq. (51) we find $V_q = 2.47$ m/sec. Using this value, together with $t_m = 4$ sec in Eq. (52) we find the criteria for the short coil to be $L^2/1.3 \times 10^4 \ll 1$. For $L = 50$ m, we find $L^2/1.3 \times 10^4 = 0.19$ which satisfies the short coil criteria. It is important to note that for the long coil case where $L = 530$ m, we find $L^2/1.3 \times 10^4 = 22$ which clearly satisfies the long coil criteria.

In Fig. 5a–b we compare the normal length and the maximum helium pressure, respectively, as obtained by the various models. The temperature dependence is not presented, since again less than 5% difference is observed between this case and Fig. 3a. The various models are in good agreement. In order to verify the dependence of X_q on L, in Fig. 6 we show the dependence of the normal length (at $t = 4$ sec) as L is varied. The y-axis is $X_q/(X_q)_r$, where $(X_q)_r$ is the normal length at $t = 4$ sec, in the case where $L = L_r = 50$

m. From Eqs. (50–51), we expect $X_q \propto 1/L^{1/3}$ in the short coil regime. This is clearly observed in Fig. 6, and as L is increased we start to enter the long coil regime, where from Eqs. (56–57) X_q becomes independent of L. The transition between the long and the short coil regimes is clearly observed in Fig. 6, and is well predicted by the analytic theory.

Small Δp Regime

This regime is very different from both the long and the short coil regimes just described which each assumed $p(t_m)/p_0 > 1$. In the long and short coil solutions we observed the same qualitative behavior in X_q, with the exception of the dependence on L. For small Δp, however, X_q is a much stronger function of L_q and J, while not dependent for example on the friction term f/d_h nor the coil length L.

In order to test the validity of the analytic solution in this region, we consider the experimental results of Ando et al. [4] which were also used in Part I [1]. These experiments fall in the "small Δp" regime as will be shown below when the pressure in the quench region is calculated. The conductor temperature for various transport currents is shown in Fig. 7a, where we compare the analytic results of Eq. (37) with those of Quencher. For this conductor $\alpha_0 = 3.9 \times 10^{-16}$ m^4-K/A^2-sec, and $T_\eta = 60$ K. The quench is initiated such that at $t = 0^+$, the value of $L_q = 0.35$ m and $T_q = 35$ K. (Note that there is a growth of the normal region beyond the initial length ($L_q(t = 0^-) = 0.04$ m) where the external heat is deposited since the value of the heat source is relatively large.) Observe that the theoretical models are in good agreement. We have plotted only the analytic and the Quencher results in order to more clearly point out the accuracy of the analytic solution. Similarly good agreement is obtained with the MacQuench model. There are no published direct experimental measurements of T to add to the comparison. In Fig. 7b, however, we compare the published experimental measurements of $2X_q$ with the analytic predictions given by Eq. (64) with $\rho_0 = 148$ kg/m^3 and $p_0 = 10$ atm. Good agreement between the analytic and the experimental results is observed, quite comparable to the comparisons with Quencher discussed in Part I [1].

We next calculate the helium pressure in the quench region for the case $I = 2$ kA ($J = 1.96 \times 10^8$ A/m^2). From Eq. (64), we find $V_q \approx R\rho_0 L_q \dot{\overline{T}}/2p_0 = R\rho_0 L_q \alpha(\overline{T}) J^2/2p_0$. At $t = t_m = 4$ sec, we find $\overline{T}$ is approximately 130 K. Using this value in Eq. (36) we find $\alpha(t_m) = 9.3 \times 10^{-16}$ m^4-K/A^2-sec. Thus, $V_q(t_m) = 1.9$ m/sec. Using this value together with $f = 0.07$, $L = 26$ m and $d_h = 6.9 \times 10^{-4}$ m in Eq. (67), we find $p_1(t_m) \approx 3.7$ atm. This value agrees very well with the pressure rise of 3.3 atm observed from the Quencher results for this case. Also note that since $p_1(t_m)/p_0 \lesssim 1$ this coil is in the small Δp regime.

6. Conclusion

A set of analytic solutions for the problem of quench propagation in CICC has been presented. These analytic solutions represent the first such results that remain valid for the long time scales of interest during a quench process. Important analytic scalings are verified by direct comparisons with numerical as well as experimental data. The analysis presented in the paper distinguishes three different regimes of operation for quench events. Each of these regimes is shown to have very distinct quench propagation characteristics. We suggest that to properly interpret any experimental results on quench propagation, it is vital to clearly distinguish the regime of operation of the magnet (e.g. distinction between long and short coils is specially important in trying to extrapolate experimental test coil results to long coils).

Acknowledgments

The authors would like to thank the members of the Engineering Division at MIT's Plasma Fusion Center for many useful discussions during the course of the work. Several engineers are specifically acknowledged for their detailed and helpful suggestions: E. A. Chaniotakis, J. McCarrick, J. Minervini, D. B. Montgomery, R. Pillsbury, J. Schultz, and R. Thome.

This work was supported by the US Department of Energy under Grant C88-110982-TKP-154-87.

References

[1] Shajii, A. and Freidberg, J. P., submitted for publication in Journal of Applied Physics, 1994.

[2] Dresner, L., 11th Symposium on Fusion Engineering, Proceedings Vol. 2, IEEE, New York, 1986.

[3] Shajii, A., "Theory and Modelling of Quench in Cable In Conduit Superconducting Magnets," Ph.D. Thesis, Department of Nuclear Engineering, Massachusetts Institute of Technology, 1994.

[4] Ando, T., Nishi, M., Kato, T., Yoshida, J., Itoh, N., Shimamoto, S., Advances in Cryogenic Engineering, Vol. 35, Plenum Press, New York, 1990.

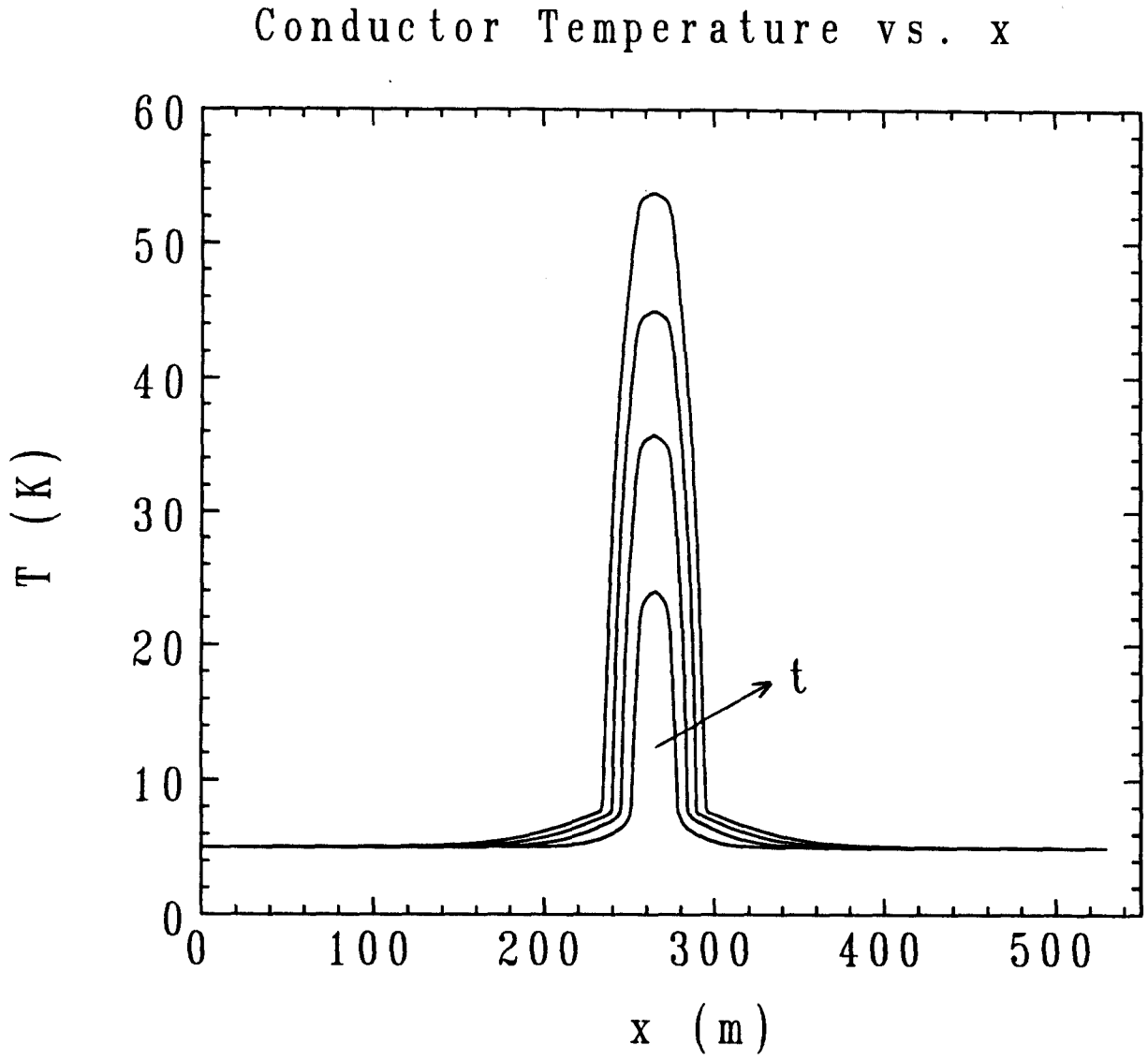

Figure 1a: Calculated conductor temperature profile during a quench in CICC.

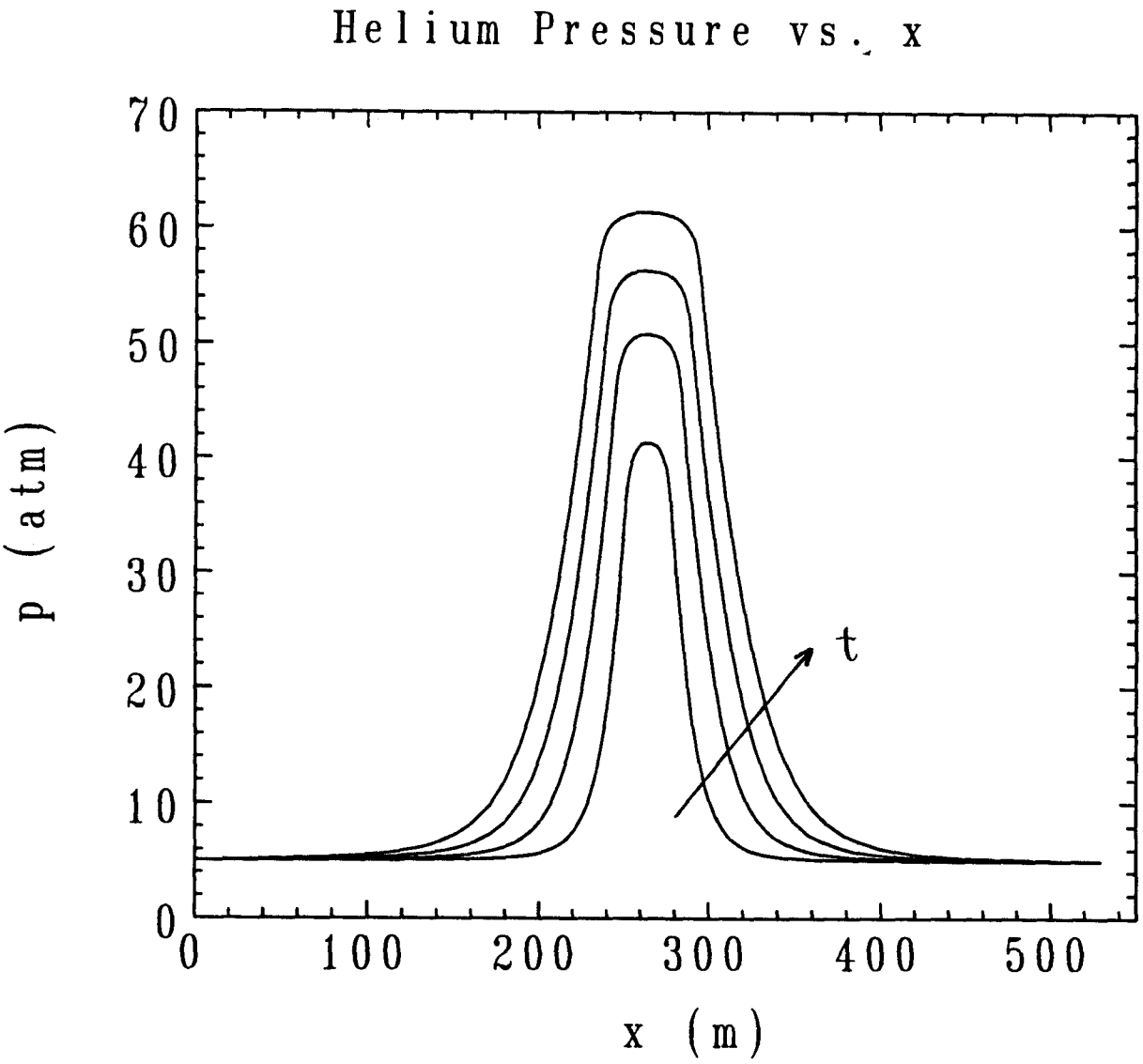

Figure 1b: Calculated helium pressure profile during a quench in CICC.

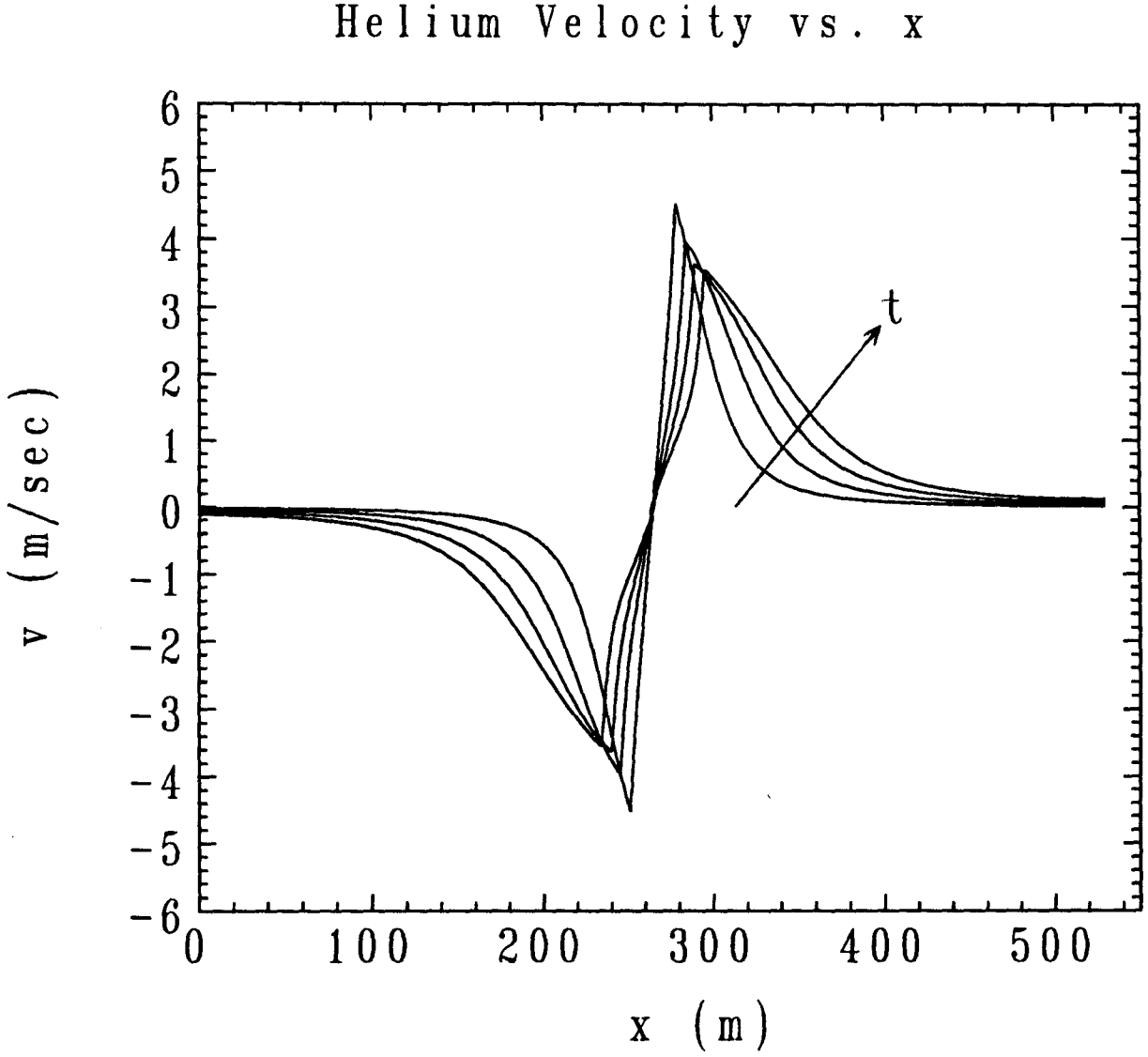

Figure 1c: Calculated helium velocity profile during a quench in CICC.

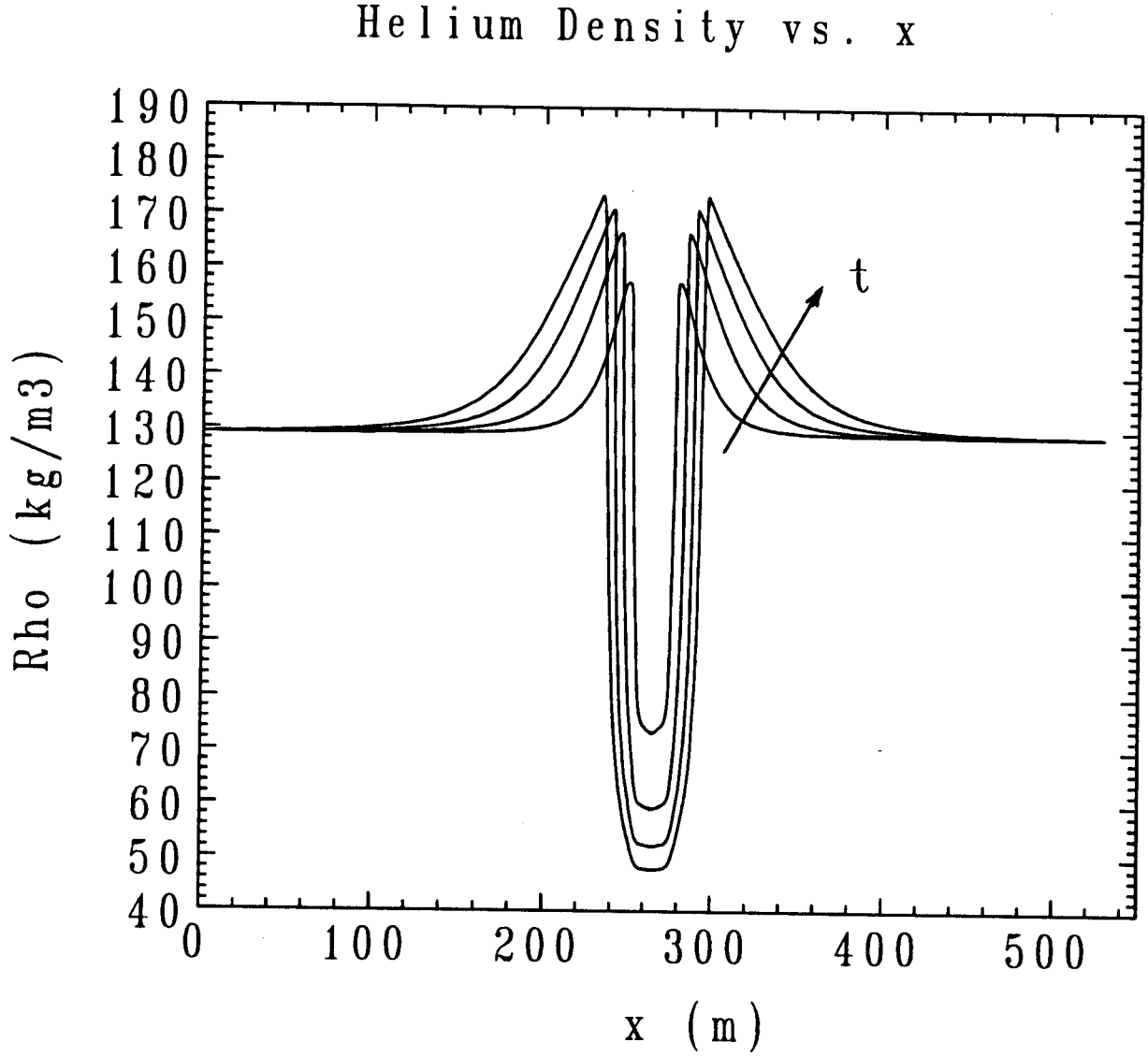

Figure 1d: Calculated helium density profile during a quench in CICC.

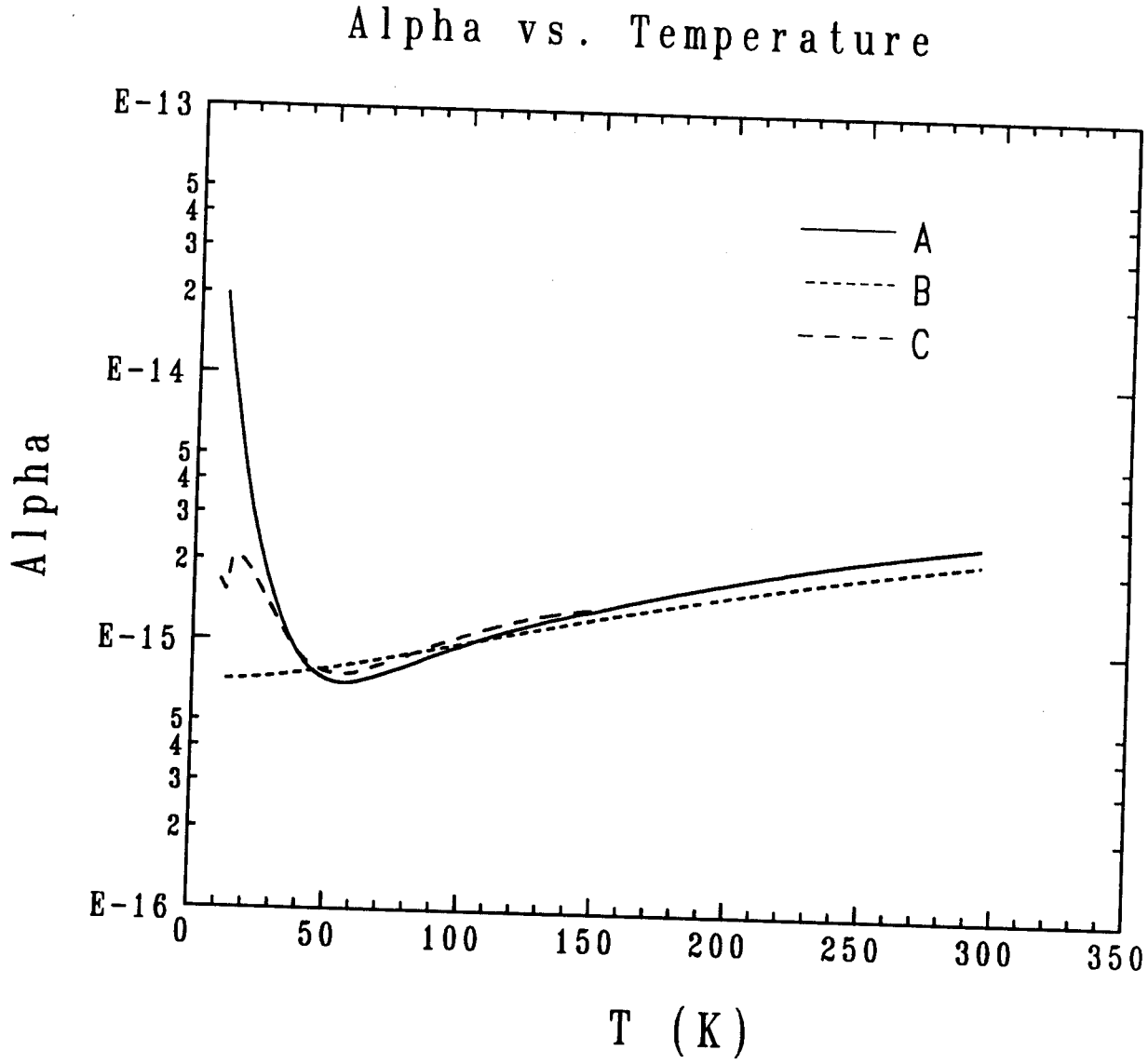

Figure 2: The parameter α as given by the following: (A) Eq. (35), (B) Eq. (36) and (C) including the helium specific heat contribution in Eq. (35).

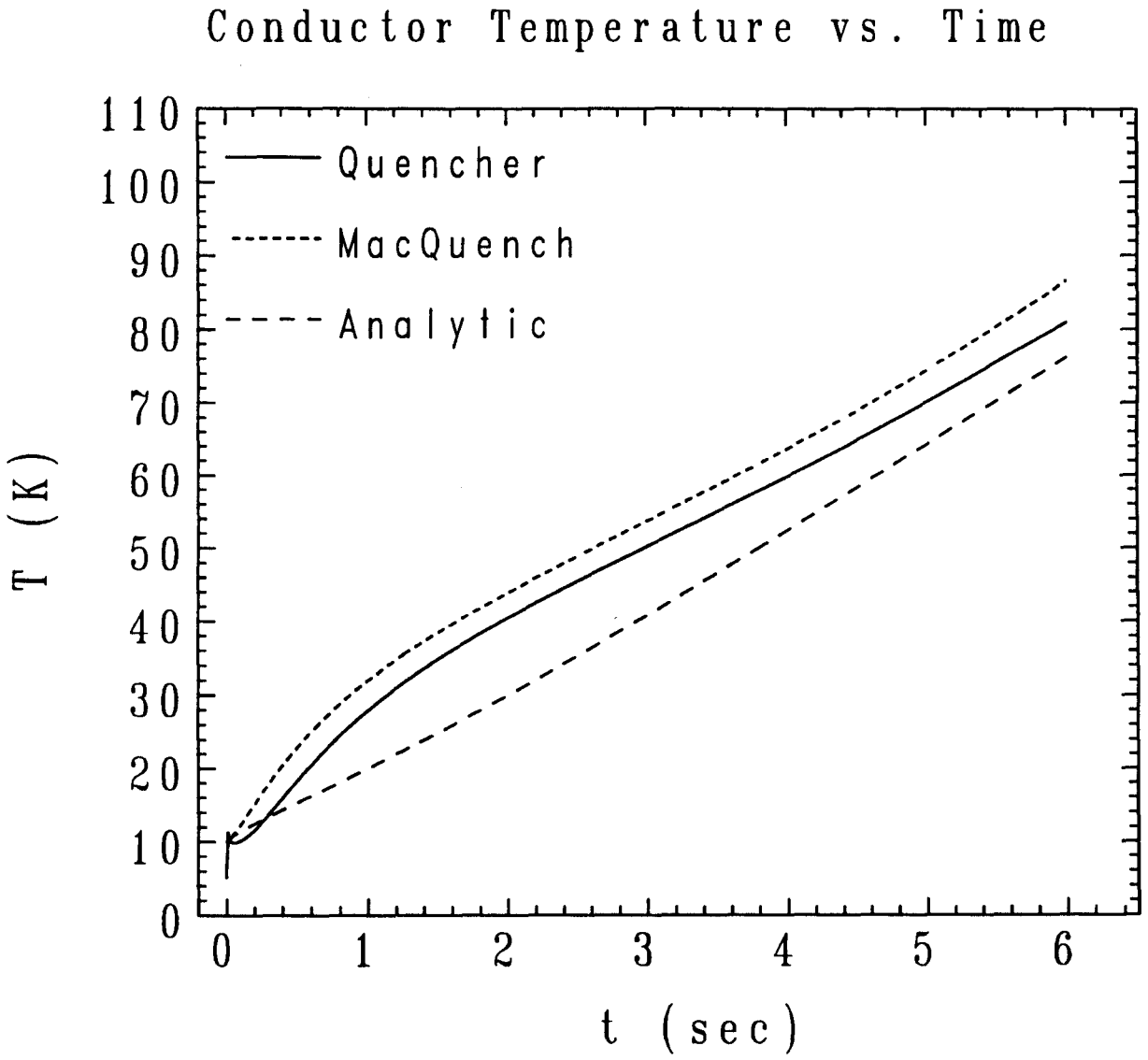

Figure 3a: Comparison of the maximum conductor temperature in a long coil as obtained by the various models.

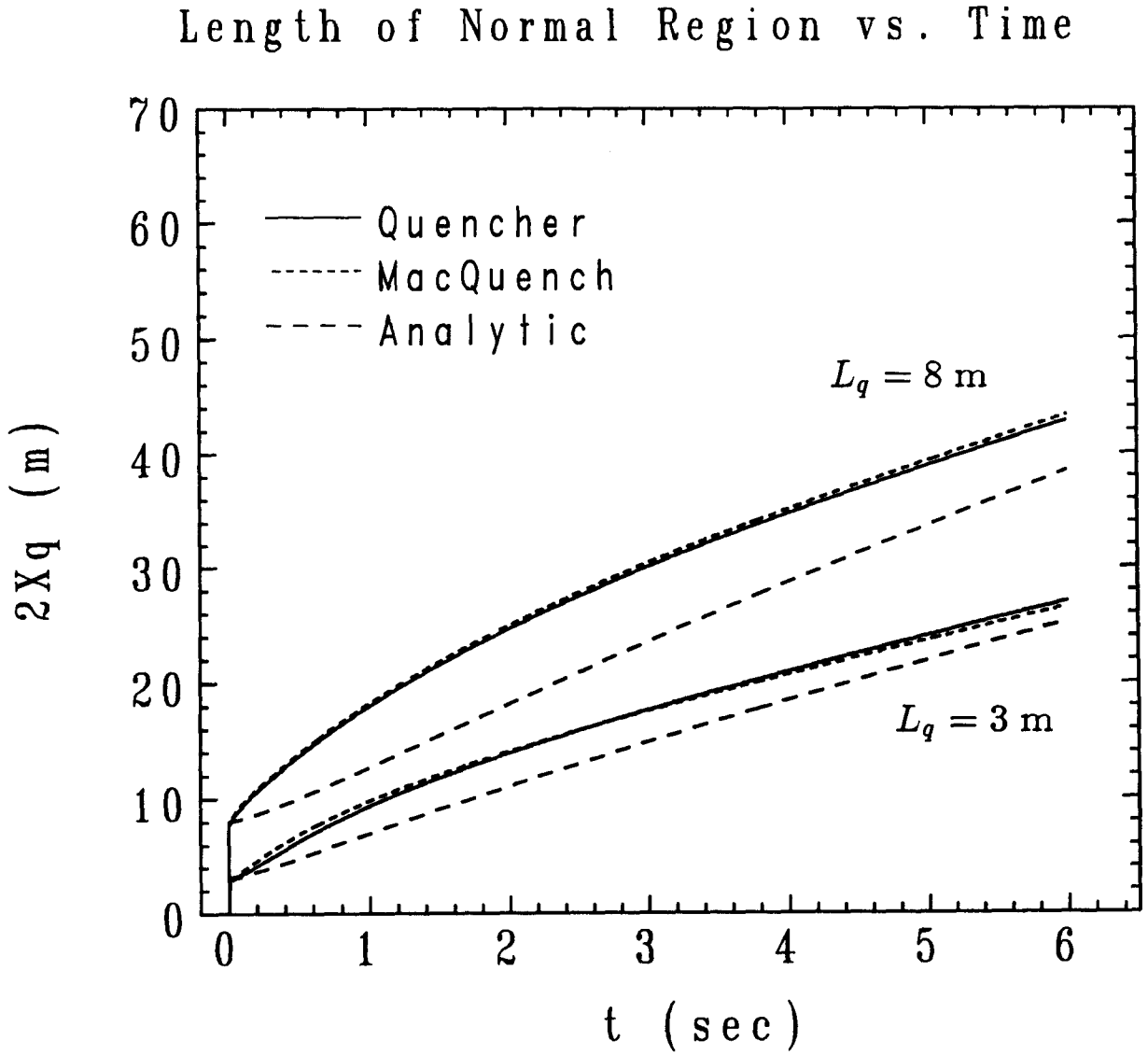

Figure 3b: Comparison of the length of the quench region in a long coil as obtained by the various models.

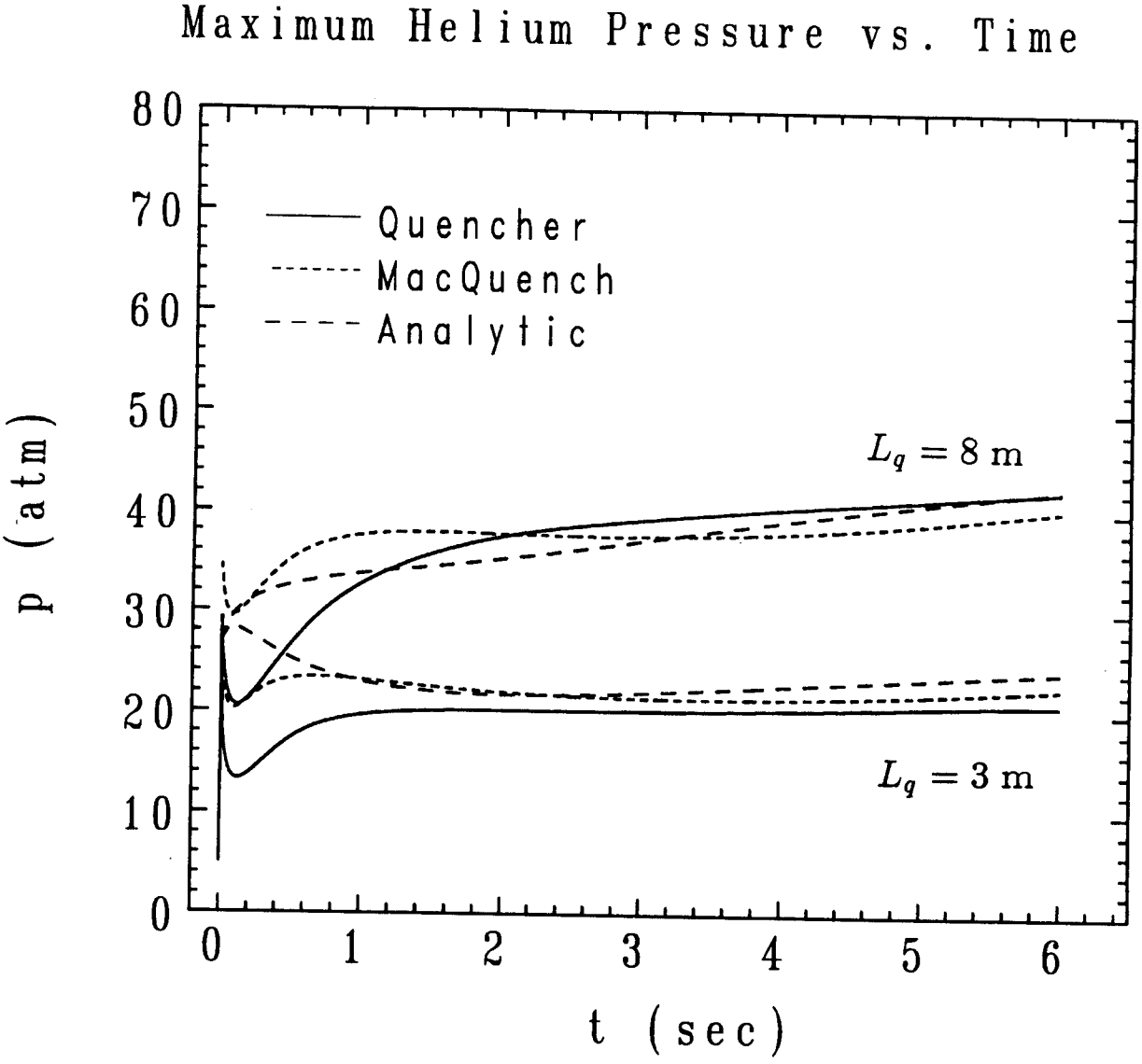

Figure 3c: Comparison of the maximum helium pressure in a long coil as obtained by the various models.

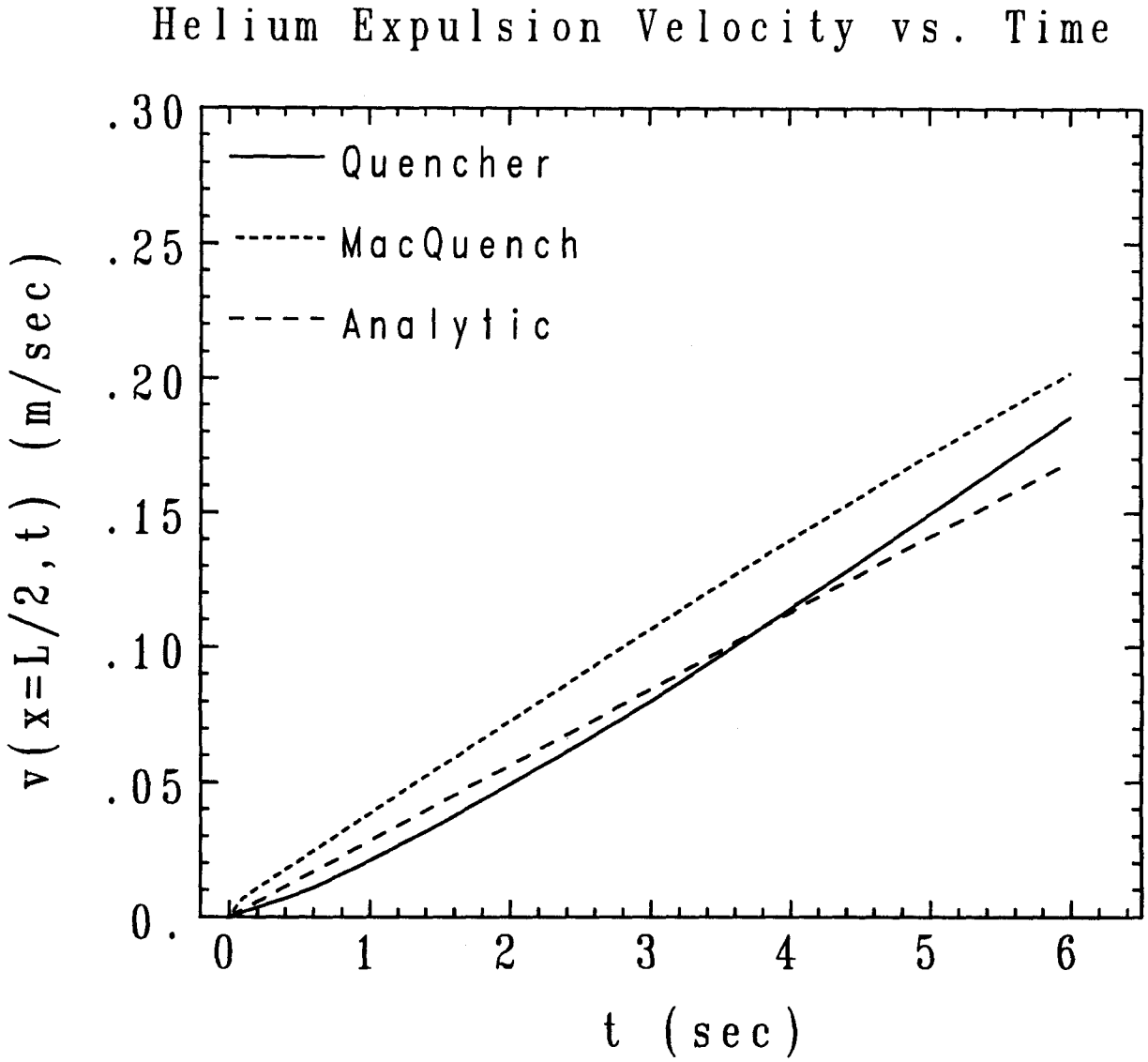

Figure 3d: Comparison of the helium expulsion velocity in a long coil as obtained by the various models.

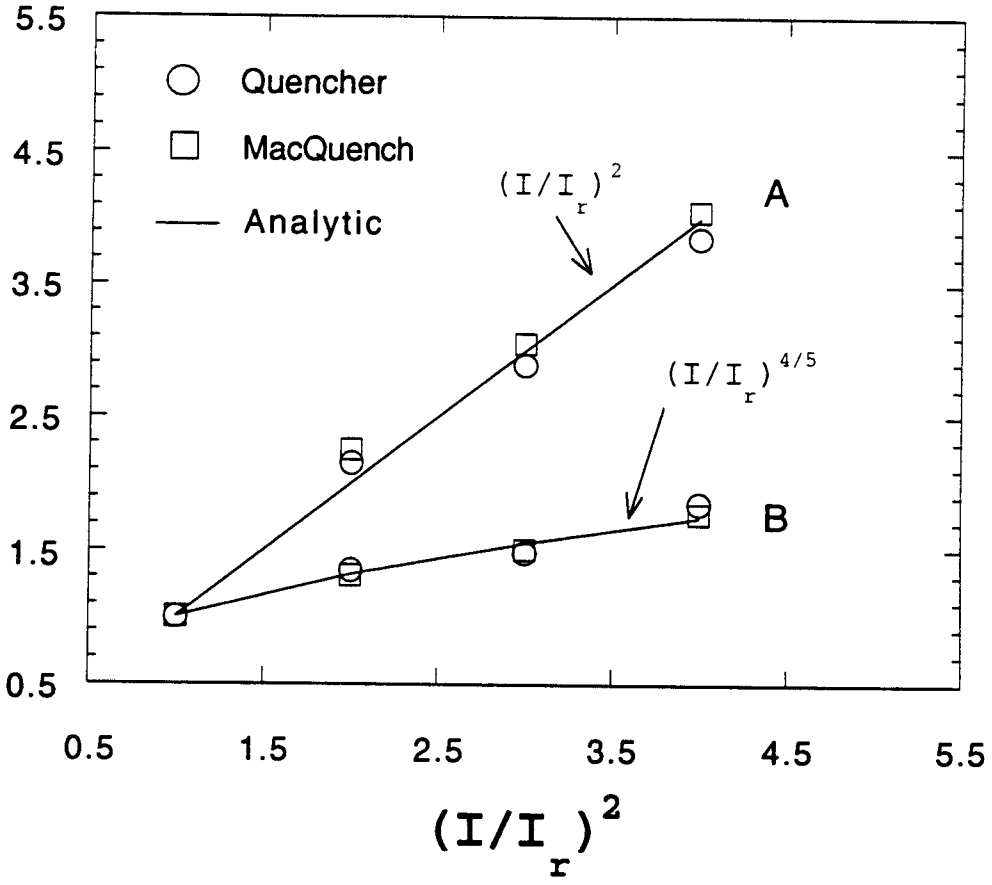

Figure 4: Comparison of $(\overline{T} - T_q)$ and $2X_q$ versus I^2 as obtained by the various models.

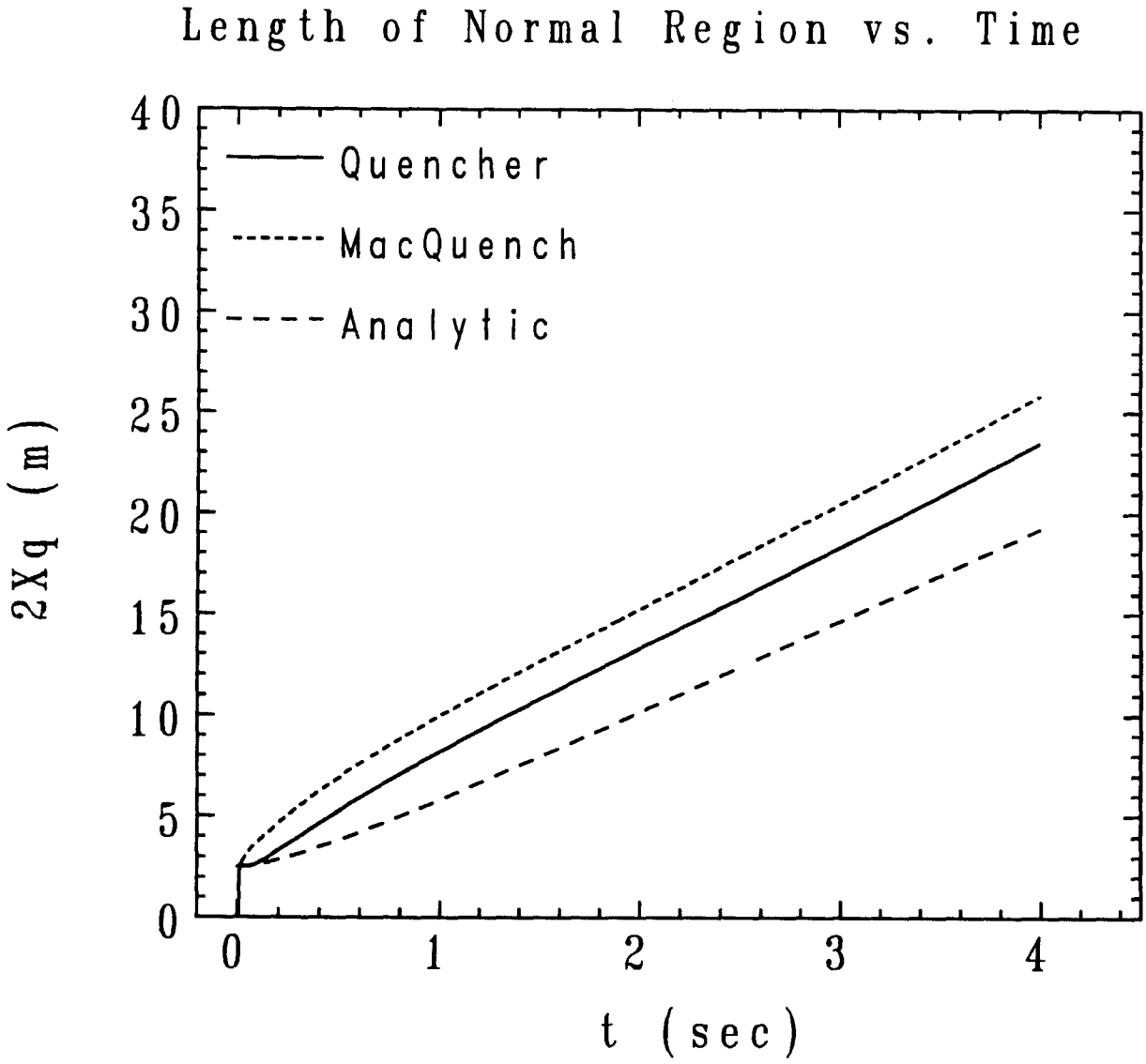

Figure 5a: Comparison of the length of the normal region in a short coil as obtained by the various models.

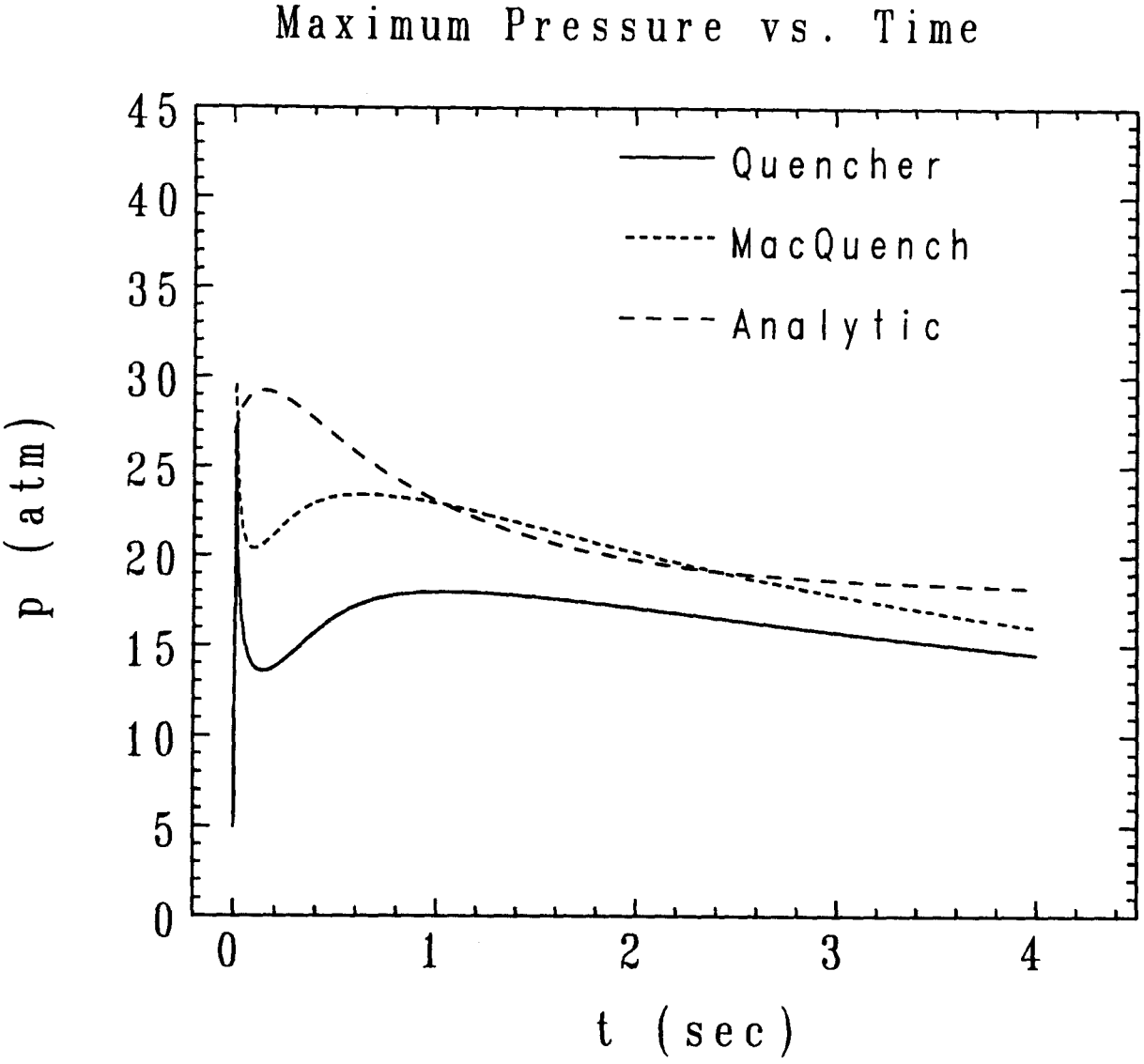

Figure 5b: Comparison of the maximum helium pressure in a short coil as obtained by the various models.

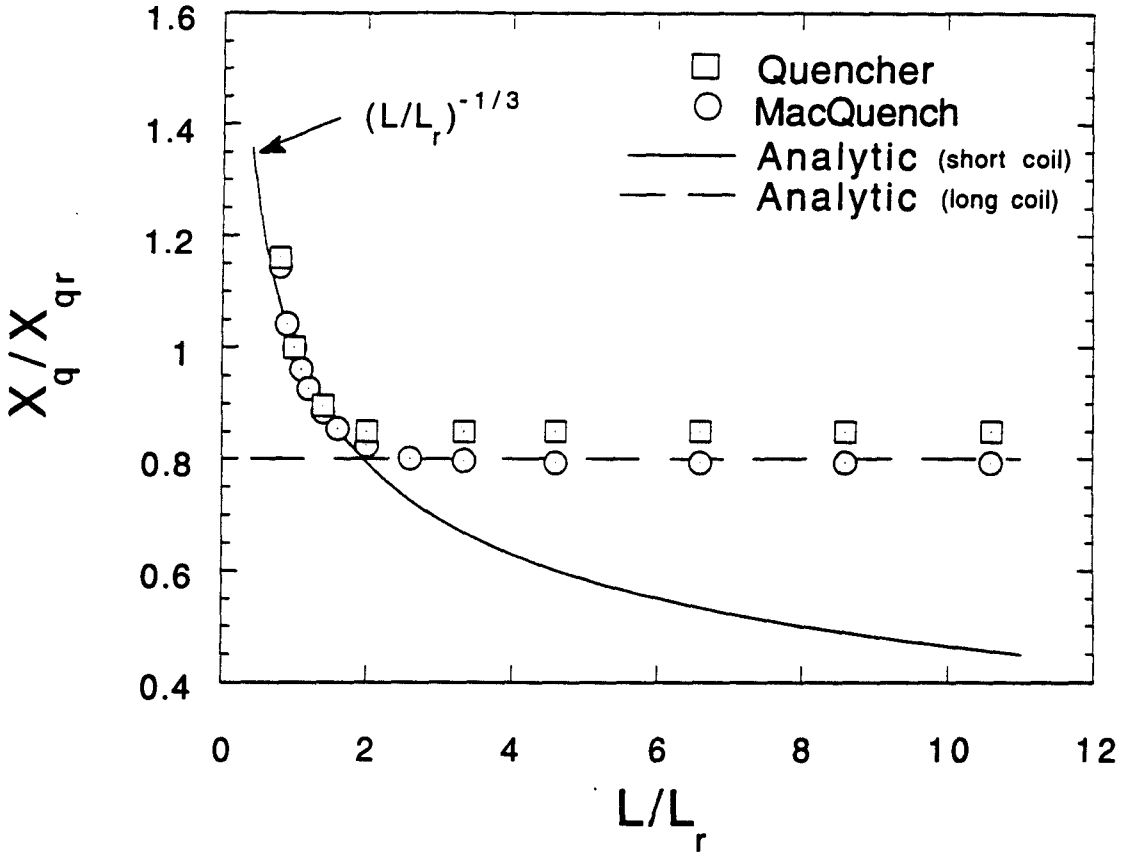

Figure 6: Comparison of the length of the normal region versus the length of the conduit, as obtained by the various models.

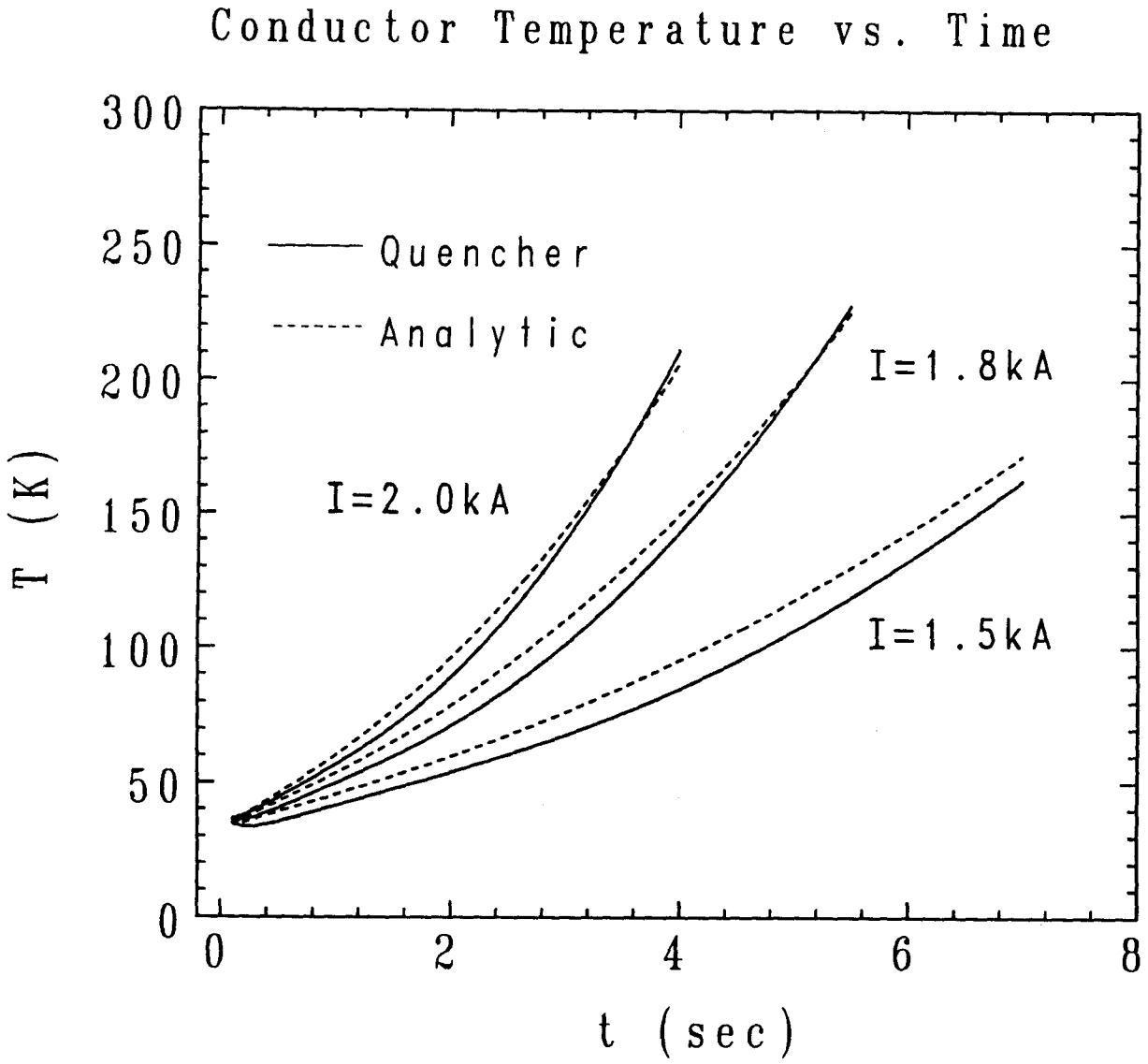

Figure 7a: Comparison of the conductor temperature in a small-Δp regime, as obtained by Quencher and the analytic results.

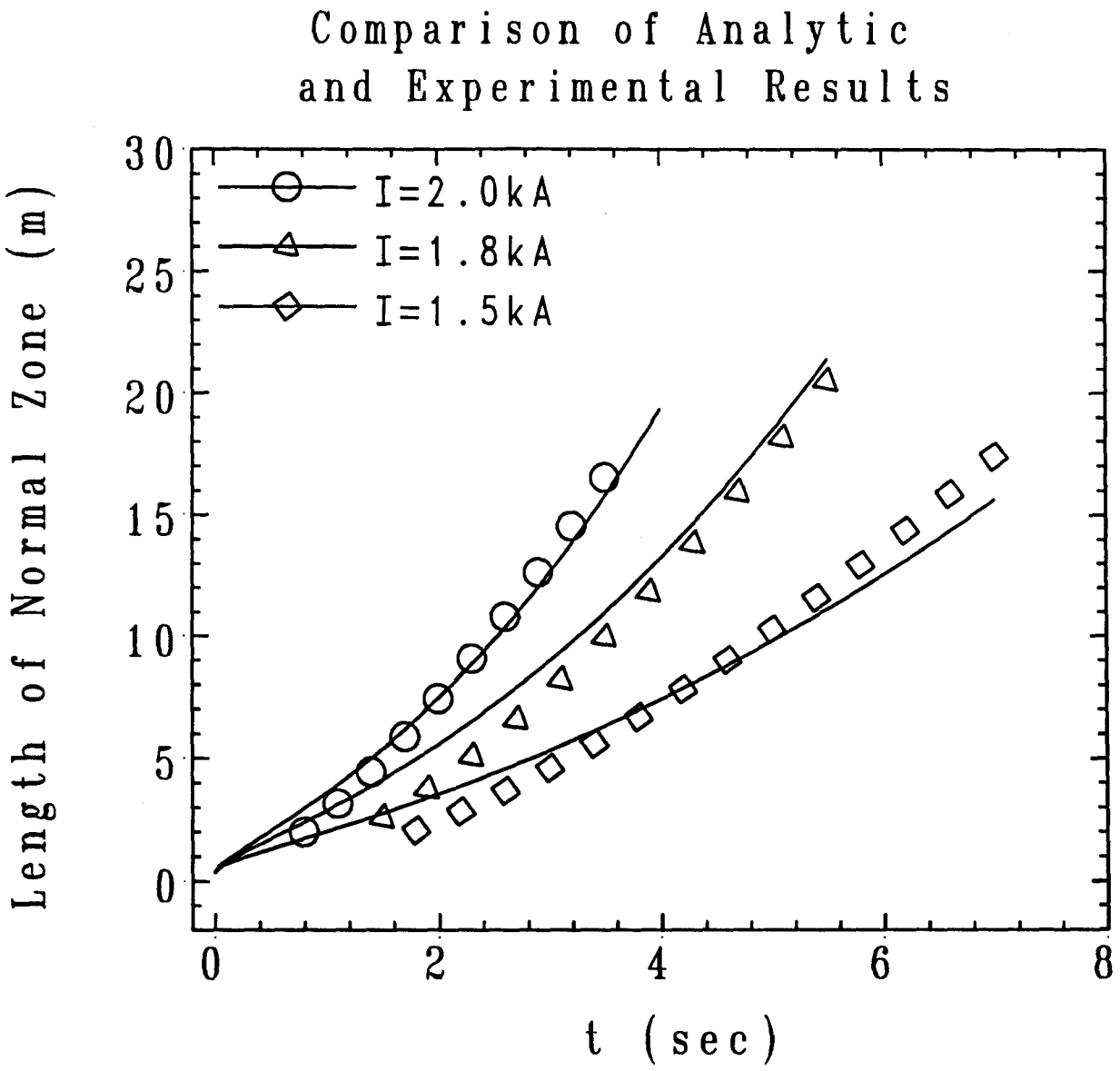

Figure 7b: Comparison of the length of the normal region as obtained by experiments of Ando et al. [4] and the analytic results.